To the Graduate Council:

I am submitting herewith a thesis written by R A Kumar entitled "Adhesion Enhancement of Metal Films Deposited Onto Excimer Laser Treated Ceramic Substrates". I have examined the final copy of this thesis for form and content and recommend that it be accepted in partial fulfillment of the requirements for the degree of Master of Science with a major in Metallurgical Engineering.

Anthony J. Pedraza, Major Professor

We have read this thesis
and recommend its acceptance:

D. H. Lowndes

Roberto Benson

Accepted for the Council:

Associate Vice Chancellor
and Dean of the Graduate School

# ADHESION ENHANCEMENT OF METAL FILMS DEPOSITED ONTO EXCIMER LASER TREATED CERAMIC SUBSTRATES

A Thesis
Presented for the
Master of Science
Degree
The University of Tennessee, Knoxville

R.A.Kumar
December, 1994

## DEDICATION

This thesis is dedicated to my parents, Ramani and A.Rajagopalan, who have been a source of inspiration, strength and guidance to me.

## ACKNOWLEDGMENTS

I wish to thank my major professor, Dr. A.J.Pedraza, for his continued guidance, support and encouragement throughout the course of my research. I am also thankful to Dr. D.H.Lowndes and Dr.R.Benson for their efforts as my thesis committee members.

I wish to thank my group members, especially Dr.M.J.DeSilva, for helping me out with the laser irradiations and for giving me invaluable suggestions. I thank Dr. Siqi Cao for his ideas and innovations in the lab and his help with the Scanning Electron Micro graphs. I also thank Mr.Jaewon Park for his constructive criticisms and discussions.

Thanks are also due to a number of people at UT, Knoxville, especially, Dr. J.E.Spruiell, for providing me with a teaching assistantship during the course of my Masters. I also thank Mr. Frank Holiway and Ms. Aileen Cagle for helping me get the required materials for my research.

Thanks are also due to a number of people at ORNL, especially, Dr.D.H.Lowndes at the Solid State Division, for letting me use the laser facility and to Mr. Sunil Abraham, Metals and Ceramics, for helping me use the SEM facility at HTML.

## ABSTRACT

The effects of pulsed excimer-laser irradiation prior to film deposition on the adhesion strength of gold, nickel or copper films sputter deposited onto polished polycrystalline alumina substrates and high purity amorphous fused silica have been studied. The effects of oxygen content of the laser irradiation atmosphere as well as the effects of thermal annealing of the metal-ceramic couples following film deposition also have been investigated. The adhesion strengths thus obtained have been correlated with scanning electron microscopy (SEM). The stability of thin films annealed at high temperatures was investigated using in-situ resistivity measurements. Adhesion enhancement of gold-alumina couples has been obtained for laser energy densities both above and below the melting threshold for alumina. The adhesion strength that results from alumina at these energy levels is associated here with the surface damage that the photo-induced sputtering generates. It is proposed that, owing to the damage, the gold or nickel atoms arriving at the surface can find bonding sites.[1] Post-deposition annealing is required for further bonding enhancement, suggesting that further rearrangement of the gold and nickel and/or oxygen and aluminum must take place to attain bonding configurations. These results are similar to those obtained

by other authors in sapphire specimens sputtered with 500 eV $Ar^+$ ions prior to deposition of copper films.[2] Fused silica, which unlike alumina is a more covalently bonded ceramic, shows different results with respect to adhesion enhancement. It does not exhibit the dramatic improvement in adhesion found with alumina, nor does it show the strikingly similar functional dependence of adhesion strength on laser energy density as obtained with alumina-gold couples. However, ablation seems to have a deleterious effect on the adhesion strength in the cases of both fused silica and alumina. It is probable that ablation removes some of the favorable conditions created for bonding by laser melting and solidification, thus accounting for decrease in adhesion strength for energy densities greater than the ablation threshold.

## TABLE OF CONTENTS


| CHAPTER | PAGE |
|---|---|
| 1. INTRODUCTION | 1 |
| 2. LITERATURE REVIEW | 5 |
| 2.1 Ceramics in Micro-electronic Packaging | 5 |
| 2.2 Laser Beam Interaction with Materials | 10 |
| 2.2.1.Optical Analysis of UV Laser interaction | 13 |
| 2.2.2.Thermal Analysis of UV Laser interaction | 16 |
| 2.3 Properties of Metal-Ceramic couples | 18 |
| 2.3.1.Thermal Properties | 19 |
| 2.3.2.Dielectric Properties | 20 |
| 2.3.3.Adhesion Properties | 21 |
| 2.4 Thin Film Deposition | 28 |
| 2.4.1.Chemical Vapor Deposition | 28 |
| 2.4.2.Physical Vapor Deposition | 28 |
| 2.5 Adhesion Tests | 32 |
| 2.5.1.Shear Test | 32 |
| 2.5.2.Tensile Test | 34 |
| 2.5.3.Scratch Test | 36 |
| 3. EXPERIMENTAL | 38 |
| 3.1 Substrates Used | 38 |
| 3.2 Laser Irradiation | 38 |
| 3.3 Thin Film Deposition | 40 |
| 3.4 Pull Testing | 41 |

3.5 Annealing Treatments.....43

3.6 In-situ Resistivity Measurements .....43

**4. RESULTS**.....47

4.1 Adhesion Testing.....47

4.1.1. Alumina-Gold.....47

4.1.2. Alumina-Nickel.....52

4.1.3. Silica-Gold.....57

4.1.4. Silica-Copper.....57

4.2 Electrical Resistance Measurements..... 59

4.3 Scanning Electron Micro graphs..... 64

4.4 In-situ Resistivity Measurements..... 74

**5. DISCUSSIONS**.....77

5.1 Laser Enhanced Adhesion..... 77

5.2 Microstructure of Metallic Films Deposited on Ceramic Substrates..... 82

5.3 In-situ Resistivity Experiments..... 86

**6. CONCLUSIONS**.....88

**REFERENCES**.....92

**VITA** .....100

## LIST OF TABLES

**TABLE** **PAGE**

2.1. Current applications of Ceramic Materials..... 6

2.2. Properties of Conventional Electronic Materials..... 9

4.1. Resistance (in KΩ) of a 20-nm thick gold film ion-beam sputter deposited onto an alumina substrate and then subject to a post-deposition annealing at 550 °C for 45 minutes..... 60

## LIST OF FIGURES

**FIGURE** **PAGE**


2.1. Reflectance and Absorption Coefficient as a function of wavelength for metals..... 12

2.2. Reflectance and Absorption Coefficient as a function of wavelength for crystalline Quartz..... 14

3.1. Schematic of the laser equipment setup..... 39

3.2. Schematic of the pull-testing apparatus..... 42

3.3. Schematic of the set-up of the annealing of metal-ceramic couples..... 44

3.4. Schematic of the in-situ resistance experiment..... 46

4.1. Adhesion strength of gold-alumina couples as a function of laser energy density. The alumina substrates were laser treated in $Ar/H_2$..... 49

4.2. Adhesion strength of gold-alumina couples as a function of laser energy density. The alumina substrates were laser treated in air..... 50

4.3. Adhesion strength of gold-alumina couples as a function of laser energy density. The alumina substrates were laser treated in oxygen..... 51

4.4. Adhesion strength of gold-alumina couples as a function of laser energy density. The alumina substrates were laser treated in three different atmospheres..... 53

4.5. Adhesion strength of gold-alumina couples as a function of laser energy density. The alumina substrates were laser treated in three different atmospheres and the couples were subjected to a 300 °C post-deposition annealing..... 54

4.6. Adhesion strength of nickel-alumina couples as a function of laser energy density. The alumina substrates were laser treated in $Ar/H_2$..... 55

4.7. Adhesion strength of nickel-alumina couples as a function of laser energy density. The alumina substrates were laser treated in air..... 56

4.8. Adhesion strength of gold-silica couples as a function of laser energy density. The silica substrates were laser treated in three different atmospheres and the couples were subjected to a 300 °C post-deposition annealing..... 58

4.9. Adhesion strength and resistance as a function of laser energy density. The laser irradiations were carried out in a reducing atmosphere,i.e.$Ar/H_2$..... 61

4.10. Adhesion strength and resistance as a function of laser energy density. The laser irradiations were carried out in air..... 62

4.11. Adhesion strength and resistance as a function of laser energy density. The laser irradiations were carried out in oxygen..... 63
4.12. SEM micro graph of a 20-nm thick gold film sputter deposited on an alumina substrate laser treated in $Ar/H_2$ at 2 $J/cm^2$ and then subjected to a 550 °C post-deposition annealing for 45 minutes..... 65
4.13. SEM micro graph of a 20-nm thick gold film sputter deposited on an alumina substrate laser treated in air at 2 $J/cm^2$ and then subjected to a 550 °C post-deposition annealing for 45 minutes..... 66
4.14. SEM micro graph of a 20-nm thick gold film sputter deposited on an alumina substrate laser treated in oxygen at 2 $J/cm^2$ and then subjected to a 550 °C post-deposition annealing for 45 minutes..... 67
4.15. SEM micro graph of a 20-nm thick gold film sputter deposited on an as-received alumina substrate and then subjected to a 550 °C post-deposition annealing for 45 minutes..... 68
4.16. SEM micro graph of a 20-nm thick gold film sputter deposited on an alumina substrate laser treated in air at 0.5 $J/cm^2$ and then subjected to a 550 °C post-deposition annealing for 45 minutes..... 69
4.17. SEM micro graph of a 20-nm thick gold film sputter deposited on an alumina substrate laser treated in air at 1 $J/cm^2$ and then subjected to a 550 °C

post-deposition annealing for 45 minutes..... 70
4.18. SEM micro graph of a 20-nm thick gold film sputter deposited on an alumina substrate laser treated in air at 2 J/cm$^2$ and then subjected to a 550 °C post-deposition annealing for 45 minutes..... 71
4.19. SEM micro graph of a 20-nm thick gold film sputter deposited on an alumina substrate laser treated in air at 3 J/cm$^2$ and then subjected to a 550 °C post-deposition annealing for 45 minutes..... 72
4.20. SEM micro graph of a 20-nm thick gold film sputter deposited on an alumina substrate laser treated in oxygen at 1 J/cm$^2$ and then subjected to a 550 °C post-deposition annealing for 45 minutes..... 73
4.21. Resistance changes in a 200 °A gold film deposited on as-received alumina and alumina laser treated in oxygen at 1 J/cm$^2$..... 75
4.22. Resistance changes in a 600 °A gold film deposited on alumina laser treated in oxygen at 1 J/cm$^2$ and 3 J/cm$^2$..... 76

# CHAPTER 1

# INTRODUCTION

Metal films that are strongly bonded to insulators are widely needed for use in microelectronics, magnetic and optical devices, and protective coatings. In microelectronics, a strong metal-insulator bond is vital for reliability of large scale integrated circuits.[3] In fact, usually, it is the strength of the interfacial bonding which limits the use of particular metal-ceramic couples. In this investigation, the effects of pulsed excimer laser irradiation of polycrystalline alumina and amorphous fused silica substrates on the bonding with subsequently sputter deposited gold, nickel or copper films have been studied. Excimer lasers are able to deliver an intense and localized energy to the workpiece. Materials processing with this type of laser can be performed at high speed, excellent reproducibility and process control, and without the need of high vacuum.[4]

Polycrystalline ceramics, notably alumina ( polycrystalline aluminum oxide, p-$Al_2O_3$ ) , are widely used in the electronics industry as substrates for metal-film deposition, as well as in other industrial applications that require metal-ceramic bonding. For electronic applications a very smooth surface finish is desired in order to reduce metallization thickness and to place thin, metal lines to be

placed close together.[5] Although ceramic substrate manufacturers strive for surface uniformity and an uniform grain structure, the fundamental limit on surface smoothness is the grain size itself. Voids exist between grains, resulting in an irregular surface profile, with two very important consequences: 1) very poor adhesion strength of subsequently deposited metal films like gold, copper or nickel and 2) the necessity to use thicker, widely separated metallization than would be required on a perfectly smooth substrate or in other words, very poor resolution in the metallization of these substrates. Multi-shot pulsed XeCl (308 nm) excimer laser irradiation has been found to melt a 0.2 μm-thick near-surface region of commercial fine grained alumina substrates at a laser energy density of $1J/cm^2$.[6] The melted alumina substrate becomes smoother because the molten alumina flow tends to spread uniformly. Not only a significantly smoother surface finish is obtained, but also the bonding strength of subsequently deposited copper films to the laser treated alumina surface is increased by a factor of 3 to 5 under optimum laser conditions. Ablation takes place at higher energy densities; for instance, at $2J/cm^2$ the ablation rate is 27 nm per pulse.[5] A relevant feature of the ablation in alumina is that material removal starts only after a threshold number of pulses, e.g. , five pulses are required to initiate ablation at $2\ J/cm^2$ . As the laser energy density increases, the threshold number of pulses for

ablation decreases. The initiation of ablation of fused silica takes place at a much higher energy density or with a greater threshold number of pulses, e.g., twenty pulses are required to initiate ablation at 2 $J/cm^2$ and at least ten pulses to initiate ablation at 3 $J/cm^2$ . But after the onset of ablation, subsequent material removal is comparable to alumina, e.g., the ablation rate is 20 nm per pulse at 2 $J/cm^2$. The interaction between several wide-band gap materials and the ultraviolet electromagnetic radiation is likely to be mediated by defects and impurities.[7] The detected threshold number of pulses can then be related to the generation of significant damage in order to couple the near surface region of the ceramic to the laser beam. The incubation period is much shorter for polycrystalline alumina substrates [5] than for either single crystal sapphire or high purity fused silica because the alumina substrates contain an uniform high density of "native defects" that strongly couple with even an initial laser pulse. These defects are grain boundaries, irregular crystalline facets that exist on the micrometer scale and trace impurities. The laser irradiation itself produces point defects, like vacancies and interstitials, which can be important for increasing bonding to metallic films. The defective surface may therefore contain sites where the metal atoms can be placed and a strong bonding can be created. Under this assumption, the adhesion strength should be proportional to

the number of anchored atoms on those defective lattice sites.

The oxygen content of the atmosphere in which laser irradiation is carried out also influences the adhesion strength. Even for a non-reactive metal like gold ( with the heat of formation of $Au_2O_3$ being +39 Kcal/mol ), [8,9] oxygen seems to play a vital role in subsequent adhesion of gold to the ceramic substrates, particularly alumina. Moore and Thornton [10] showed that a very strong bonding was developed when gold was melted in fused silica under the presence of oxygen. If oxygen was not present during the melting, the bonding of the gold droplet to silica was very weak. Mattox [11] observed that by having oxygen present in the gas discharge during triode sputtering of gold films on fused silica surfaces, it was possible to increase the adhesion of gold-silica couples without any intermediate material. In sapphire and alumina substrates irradiated in air, [12] it has been found by X-ray photoelectron spectroscopy, that the amount of oxygen present in the near surface is higher than the stoichiometric ratio. Oxygen, also has a stabilizing effect on thin tin films by delaying agglomeration of the film during annealing. As reported by Caswell and Budo, [13] any stage in the metamorphosis of a thin tin film from an initially flat and continuous structure at lower temperature to an agglomerated, lacy structure at higher temperatures can be obtained by "fixing" the film in oxygen.

# CHAPTER 2

# LITERATURE REVIEW

## 2.1 Ceramics in Micro-electronic Packaging

Ceramics are defined as complex inorganic compounds and solutions containing both metallic and non-metallic elements, which are joined together by ionic or covalent bonds. They are typically hard, brittle, high melting point materials with good chemical and thermal stability and high compressive strengths. Ceramics have been an integral part of the information-processing industry as they make it possible to store, display, print and transfer information. The materials currently being used for these applications are shown in Table 2.1. [14]

Packaging still remains as one of the most important application of ceramics in microelectronics. Ceramic packages constitute roughly 80% of the total packaging market, currently a multibillion dollar industry. Ceramics possess a combination of electrical, mechanical, thermal and dimensional properties unmatched by any other group of materials. For example, ceramics have thermal expansion coefficients matching that of Silicon ($30 \times 10^{-7}$/°C) or Copper ($170 \times 10^{-7}$/°C) , dielectric constants ranging from 4 to 10,000 and thermal conductivities that range from matching one of the best insulators to exceeding that of Aluminum metal (220 W/m.K), one of the best thermal conductors known. Ceramic

Table 2.1. Current applications of Ceramic Materials.

| **Information Technology** | **Application** | **Ceramic materials** |
|---|---|---|
| Processing<br>Package<br>Device | Substrate<br>Dielectric<br>Mask | $Al_2O_3$, BeO,SiC,AlN,<br>$Si_3N_4$, $SiO_2$<br>Borosilicate glasses |
| Storage | Disk<br>Tape<br>Head | Iron Oxide, Chrome Oxide,<br>Ferrites,Glass, $Al_2O_3$ + TiC<br>substrate |
| Display | Dielectric<br>Seal<br>Face plate | Lead Borosilicate glass,<br>Lead Zinc Borosilicate<br>glass, Soda-lime glass |
| Printing | Ink jet<br>Electroerosion | $ZrO_2$-containing glass<br>Ceramic-metal composites |
| Transfer | Optical fiber | $SiO_2$, $B_2O_3$ -$SiO_2$ |

materials in the form of dual in-line packages (DIP),chip carriers, flat-packs, and pin grid arrays are used throughout the industry, in everything from mainframe computers to consumer electronics. [15] Recent technological breakthroughs have opened the doors for ceramics to superconducters, which provide no electrical resistance to current flow. The high temperature stability of ceramic substrates is another desirable property which makes ceramic packages the only choice, especially where hermeticity is required.

On the other hand, ceramic packages suffer from the following three main drawbacks: 1) They are brittle and thus prone to catastrophic failure and sensitive to stress corrosion. 2) They require higher processing temperatures than plastics, making them more expensive. 3) They cannot match thin-film organic packages, in very high performance applications which require very low dielectric constants and high packaging densities. Nevertheless, ceramics are supposed to be the stable building blocks on which high-performance thin film wiring can be developed.

The ceramic substrates studied in this investigation are alumina and fused silica. Alumina($Al_2O_3$) is a common and useful insulator material for oxide ceramics and the electronics industry. Alumina systems have been chosen because of their high strengths , their good thermal conductivity , their well developed processing technology and

their capability to be used to make packages with highly reliable hermetic seals. They have been popular right from the time of the initial development of laminated multilayer ceramic modules , since J.L.Park patented his tape-casting technique in 1961. [16] Various ceramic modules developed by IBM , like the Solid Logic Technology (SLT) module developed in 1963, the Monolithic Systems Technology (MST) developed in 1970, Multichip Module (MCM) developed in 1979 and the Thermal Conduction Module (TCM) developed in 1985 used 90 -96 % Alumina as their substrates. However , Alumina has its disadvantages in having a low thermal conductivity and high dielectric constant, which delays switching time. Other ceramics like Aluminum Nitride and Silicon Nitride are being developed to replace the current Aluminas. Table 2.2 compares the common properties of conventional electronic materials with that of alumina.[17]

Synthetic fused silica is the material of choice for varied optical applications in the UV ( ranging from lens components for photolithography [18] to beam delivery systems in medical instrumentation [19] ), micro-optics and fiber technology. It is characterized by high transmission from the UV to the IR and outstanding thermal , electrical and chemical properties. Since conventional machining is rather difficult , excimer lasers are appropriate tools for drilling, cutting, patterning, roughening, polishing and shaping processes.

Table 2.2. Properties of Conventional electronic materials.

| Material | CTE ( $10^{-6}$ /K) | Thermal Conductivity [ W/(m.K)] | Density ($g/cm^3$) | Specific Thermal Conductivity [ W/(m.K)] |
|---|---|---|---|---|
| Silicon | 4.1 | 135 | 2.3 | 58 |
| Alumina | 6.5 | 20 | 3.9 | 5 |
| Beryllia | 6.7 | 250 | 2.9 | 86 |
| AlN | 4.5 | 250 | 3.2 | 78 |
| Aluminum | 23 | 221 | 2.7 | 82 |
| Copper | 17 | 400 | 8.9 | 45 |
| Kovar | 5.9 | 17 | 8.3 | 2 |
| Molybdenum | 5 | 140 | 10.2 | 14 |
| CIC(20/60/20) | 5.2 | 167 | 8.4 | 19 |
| Epoxy | 60 | 0.3 | 1.2 | 0.3 |

## 2.2 Laser Beam Interaction with Materials

Laser beams as well as medium-energy electron beams are currently being used in a whole range of new applications-from growing crystals to quenching alloys into metastable states, and from depositing films to purifying surfaces. All of these applications are ultimately caused by heat, as a greater part of the beam energy is absorbed by different coupling mechanisms. The absorption of laser beams in a material depends strongly upon its detailed electronic structure, which in turn is modified as a result of the irradiation. The effects of these self-induced coupling phenomena are more pronounced in laser beam irradiation as opposed to electron-beam irradiation.[20] Lasers are currently enjoying great popularity among material scientists and engineers. As versatile sources of energy in a highly concentrated form, lasers have become attractive tools and research instruments in metallurgy, semiconductor technology and engineering.[21] Laser beams can deliver concentrated energy to almost any material , and they do so exactly where, when , and in the quantity desired. Lasers are increasingly being used to modify the near-surface region without changing the properties of the bulk material. Lasers emit monochromatic and nearly coherent light and the laser beam which is almost parallel, is capable of delivering immense power. Upon impact of a laser beam on a material, electromagnetic energy is first converted into electronic

excitation , which is then transferred into thermal, chemical and mechanical energy, thereby altering irreversibly the molecular structure and the shape of the material. For metals, lasers are perfect surface heating sources in the visible or infra-red region. This is because , metals, due to the high density of free electrons in them , have large absorption coefficients (corresponding to absorption lengths $\alpha^{-1}$ around 100 'A ) . Though a large portion of this energy absorbed by the electrons is re-emitted ,the remaining portion is transferred to the lattice in a very short time ($10^{-11}$ to $10^{-12}$ s). In the UV range, the reflectivity of the metals strongly decreases. Figure 2.1 shows the absorption coefficient and the reflectivity of metals in the whole range of the spectrum.[20] Ceramic materials in the absence of excitation have only bound electrons and are basically transparent , except in the vicinity of what can be thought of as resonances. The most important resonance arises from transitions of valence bond electrons to the conduction band, also known as interband transitions. When the incident photon energy is at least equal to the band gap energy ,$E_g$ , an interband transition occurs, and the free carriers (electrons and holes) created, can, if present in sufficient numbers, influence the optical response of the material by, say, increasing the absorption coefficient. Another type of resonance occurs, in the near infra-red region, by coupling to high-frequency optical phonons characteristic of lattice

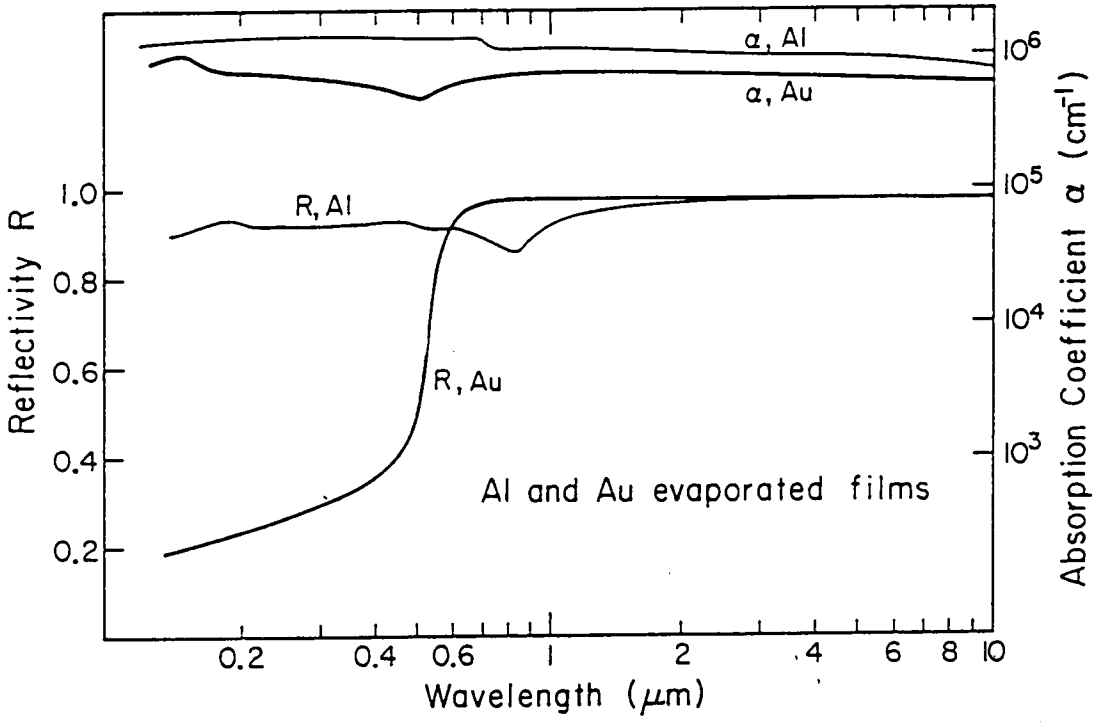


Figure 2.1. Reflectance and Absorption Coefficient as a function of wavelength for metals.

vibrations. Figure 2.2 shows the absorption coefficient and reflectance as a function of wavelength of Quartz ( $E_g$ = 6.9 eV), which shows absorption peaks around 10 mm due to phonon coupling, weak absorption at intermediate wavelengths and a steep increase in absorption as the photon energy approaches the band gap.[22] Furthermore, the optical properties are modified by light scattering at grain boundaries or inclusions. This results in quite strong absorption in ceramics, which otherwise, would have been intrinsically transparent.

The optical and thermal analysis of UV laser interaction with materials is now discussed.

### 2.2.1 Optical Analysis of UV Laser Interaction

Excimer lasers, which operate in the UV range, use noble gas-halides as a lasing medium and can produce fast pulses of durations in the order of nanoseconds. Due to their lack of coherency, they can produce uniform pulses by eliminating diffraction effects and thus can be used in materials processing. The intensities obtained are very high. Electromagnetic radiation with wavelength in the UV range, interacts exclusively with electrons, as atoms are too heavy to respond significantly to these high frequencies. ($\nu = 10^{13}$ Hz ). Therefore the optical properties of matter are determined by the energy states of either bound or free valence electrons. Bound electrons interact very weakly

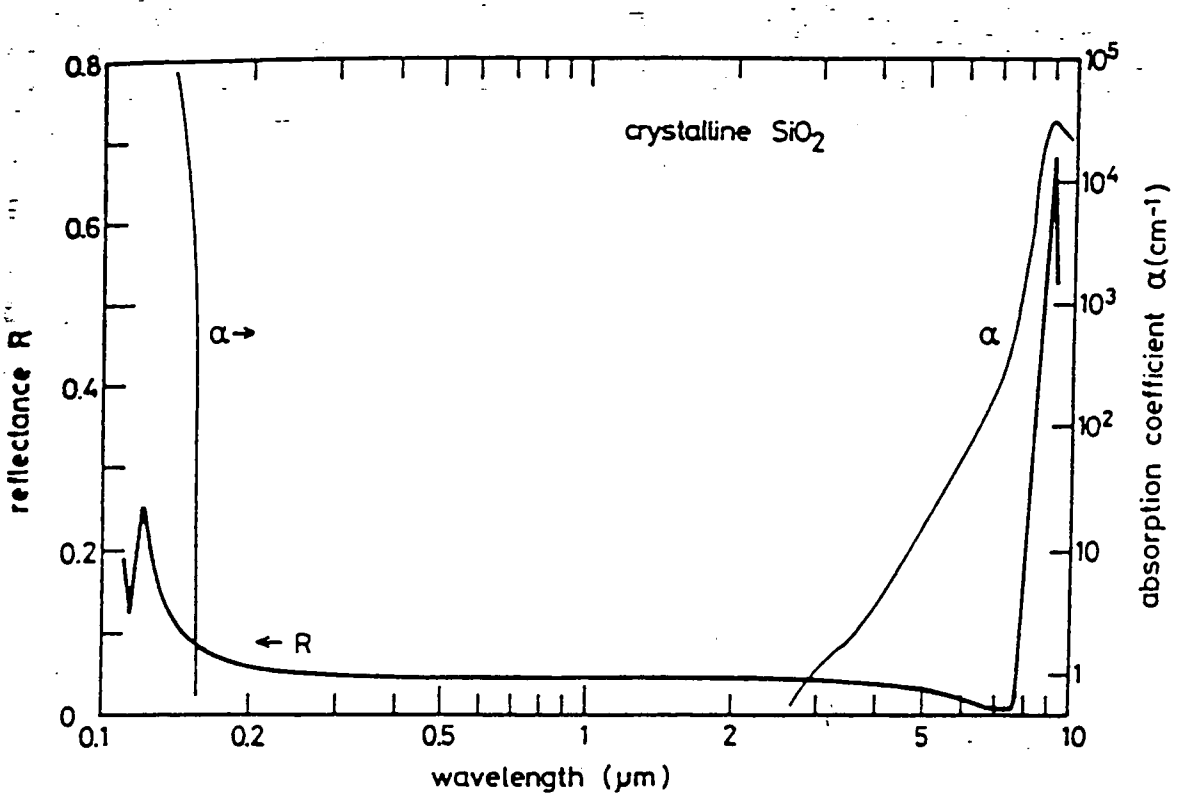


Figure 2.2. Reflectance and Absorption Coefficient as a function of wavelength for crystalline Quartz.

with the external field, changing only its phase velocity. Free electrons extract energy from the field by being accelerated by the electrical and magnetic components of the incoming field. These electrons then transfer energy to the lattice through collisions with the atoms and thus weaken the external field. However, since the field is periodically changing , the oscillating electrons also re-radiate their kinetic energy, which contributes to the reflection properties of the material. Since optical wavelengths $\lambda$, are large compared to atomic distances, the response of matter to light can adequately be described by macroscopic quantities, such as the complex refractory index, $N = n + ik$. The real part, n, is the ratio of the phase velocities in vacuum and material, and the extinction coefficient, k, describes the dampening of the electromagnetic radiation. The degree of coupling ,which is quantified by the reflectivity R, and the absorption coefficient $\alpha$ , can then be related to the above quantities by well known formulae for normal incidence,

$$R = \frac{(n-1)^2 + k^2}{(n+1)^2 + k^2}$$

and $$\alpha = (4\pi k)/\lambda$$

When a laser beam encounters the boundary between two media that have different optical properties, part of the beam is

reflected and part is transmitted. The transmitted part can be partially or totally absorbed depending upon the optical properties of the material given by the above equations. If light of intensity I is normally incident on a material surface , the power density absorbed at depth z is given by

$$\varphi(z) = I(1-R)\ \alpha\ e^{-\alpha z}\ .$$

where I is the incident power intensity, R is the reflectivity and $\alpha$ is the absorption coefficient.

### 2.2.2 Thermal Analysis of UV Laser Interaction

A model has been built according to the thermal processes where the energy of the incident laser beam is transferred to the lattice as heat in a very short time ($10^{-11}$ to $10^{-12}$ s). The heat affected depth is 1 to 2 mm and the thermal flux is normal to the irradiated surface everywhere except for a small volume corresponding to the periphery of the treated area times the heat affected depth.[4] Any linear dimension in the irradiated region (say, 0.1 to 3 mm) is two to three orders of magnitude larger than the depth of the heat affected zone and hence the thermal process is treated as a one dimensional heat conduction problem. The heat generated by the laser, $\varphi(z)$, is then included as a heat source in the Fourier equation,

$$\rho c \frac{\partial T}{\partial t} = \frac{\partial}{\partial x}(\kappa \frac{\partial T}{\partial x}) + \phi(z)$$

where $\rho$ is the density, c is the specific heat and $\kappa$ is the thermal conductivity. For films deposited on the ceramic substrates there is, first, heat conduction across the film, then heat transfer at the film/substrate interface and finally heat removal by conduction across the substrate. A computer program using the enthalpy model to simulate and keep track of the phase transformations taking place during laser processing has recently been developed by Pedraza et al.[23,24] This program takes into account the melting of the film and the substrate and also indicates when vaporization of the film starts. An intermediate layer with different thermal and thermodynamic properties was included to take into account the highly defective surface layer produced as a result of surface contamination and deformation. The variation of the different thermophysical properties of the film, intermediate layer and the substrate with temperature was also taken into account to provide a more realistic picture of the laser - material interaction. A variable grid size was used to reduce the computational time. The heat generated in the film by laser energy absorption, the heat transfer from the film to the substrate, and the enthalpy changes of the film and the substrate have been calculated using this program. Assuming an adiabatic

process, the enthalpy increase was equated to the heat generated by the laser.

## 2.3 Properties of Metal-Ceramic Couples

The range of materials incorporated in an electronic package makes interfaces between such dissimilar materials like a metal and ceramic, an important area of study. The terms electronic packaging and interconnection refer to the physical link in computers and other electronic systems between the integrated circuits or other electronic device and the outside world. An electronic package is literally a container, a black box, through which the capabilities of the circuitry inside can be accessed via some kind of interconnect, usually solder.[25] They provide electrical contact to the outside world (e.g., power and signal distribution to a printed circuit board.) [26]

The package provides mechanical and chemical protection for delicate circuitry from an environment that is often surprisingly harsh. And increasingly, the thermal properties of the package and interconnect system are important for heat distribution and dissipation. The design of reliable electronic packages involves understanding the processing and behavior of the electrical, mechanical, chemical and thermal properties of a complex system of materials. The metal-ceramic thermal, dielectric and adhesion properties will now be discussed.

### 2.3.1 Thermal Properties

The thermal conductivity and coefficient of thermal expansion of the substrate are important considerations in choosing materials for electronic packaging.

a) Thermal conductivity

The highly complex circuits developed by VLSI technology consume large amounts of power ,most of which is transformed into heat within the package. This heat must be removed to minimize device failure. The thermal conductivity of a material is governed by the frequency with which the heat transfer process encounters a scattering site or mechanism, causing disruption of the heat flow. In ceramics, vibrational energy of the atoms or phonons are mainly responsible for heat flow. If the system is a perfectly periodic structure then the phonons are described by perfectly harmonic atomic vibrations. The presence of defects in real crystals destroy the harmonicity, thereby increasing the number of defect-phonon or phonon-phonon interaction and lowering the thermal conductivity. The structural defects found in ceramic materials are predominantly point defects ( like vacancies, interstitials, substitutional atoms and isotopes), planar boundaries ( like grain boundaries,

antiphase boundaries, stacking faults and interphase boundaries ) and pores, all of which act as phonon scattering sites.[22] The point defects are the dominant phonon scattering sites for packages, which normally operate between room temperature and 200°C. At these temperatures the phonon wavelengths are ~ 1 nm and the point defects are ~ 0.3 nm , making them strong scattering sites. Four parameters contribute to the increase of thermal conductivity of a ceramic material - low atomic mass, strong interatomic bonding, high elastic modulus and low anharmonicity.[17]

b) Thermal expansion

The coefficient of thermal expansion ( CTE , $\alpha$ ) of the substrate must be close to that of the device material , otherwise thermal cycling effects could lead to failure by thermal fatigue.[27]

### 2.3.2 Dielectric Properties

The dielectric constant of the material adjacent to the metallized circuitry will dictate the delay time, as the dielectric constant is linked directly to the delay time of the circuit by the relationship :

$$t_d = \{ (\varepsilon)^{1/2} l \} / c.$$

where $t_d$ is the time delay in the signal , l is the distance the signal travels , c is the speed of light , and $\varepsilon$

is the dielectric constant.[28] This is particularly important in multilayer ceramic packages because of the long path lengths involved. Since reducing $\varepsilon$ reduces the time delay, allowing faster switching times , glass ceramics with very low $\varepsilon$ have been introduced (e.g. Cordierite , for which $\varepsilon \sim 5.0$ ). [29] Smooth surfaces which reduce the distance the signal travels , are also desirable.

### 2.3.3 Adhesion Properties

Thin films on ceramic substrates are being used in an increasingly wide range of devices for their optical, magnetic and electronic properties. However, their satisfactory performance is generally limited by their poor mechanical stability, particularly their adhesion to the substrate. Adhesion, as opposed to cohesion, is defined as the atomic or molecular interaction at the interface level between two distinct materials which allows the transfer of stress from one material to the other.[30]

The work of adhesion between two interfaces, say, a metal and a ceramic can be expressed as [31] :

$$W_{ad} = \gamma_m + \gamma_c - \gamma_{mc}$$

where $\gamma_m$ and $\gamma_c$ are the surface free energies of the metal and ceramic surfaces respectively, and $\gamma_{mc}$ is the metal-ceramic interfacial free energy. The work of adhesion, which

is a measure of the work against surface forces required to separate the metal and the ceramic, is therefore maximized when the interfacial free energy is minimized.

Under equilibrium conditions, the three surface energies are related by Young's expression for the contact angle, $\theta_{eq.}$, (34)

$$\gamma_c = \gamma_{mc} + \gamma_m \cos ( \theta_{eq.} )$$

The work of adhesion is then related to the contact angle as:

$$W_{ad} = \gamma_m \{ 1 + \cos ( \theta_{eq} ) \}$$

The adhesion strength, which is the measured force required to separate the film from the substrate does not show any direct relationship to the thermodynamic work of adhesion, $W_{ad}$. However, in general, systems that have a higher work of adhesion also show high adhesion strengths during adhesion testing.[32] Since an inverse relationship exists between the interfacial free energy, $\gamma_{mc}$, and the work of adhesion, therefore, the interfacial energy can be used as a rough indication of the adhesion strength.

The adhesion strength is strongly dependent on the adhesion test used, the strain rate, the nature of stresses on the film and the substrate during the process of testing, stress concentrations, defects and elastic or plastic

deformations in the film and the substrate. Most of the adhesion tests give comparative results by keeping most of the above factors constant. The nature and condition of the ceramic - metal interface like the presence of surface contaminants, surface roughness and the existence of intermediate compounds, itself can lead to a large variation in the observed adhesion strength.

The adhesion strength of the metal-ceramic interface is dominated by the presence of microstructural flaws and is much smaller than the theoretically calculated interatomic bonding.[33] Surface impurities or contaminants further reduce the adhesion strength. A monolayer of adsorbed gas forms on a surface in about 1 second even under vacuum ( $10^{-4}$ Pa ) conditions.[34,35] Baglin [36] studied the effects of surface contaminants on the peel strengths of thin copper films to alumina. Sputter cleaned alumina substrates were exposed to purified oxygen, purified water and purified ethanol to form respectively surfaces enriched in oxygen, water-adsorbed alumina and hydrocarbon adsorbed alumina. It was found that samples exposed to purified oxygen had the highest peel strength while samples cleaned in ethanol had practically zero peel strength.

The formation of an intermediate compound at the interface also strongly influences the adhesion properties. Pepper[37,38] measured the contact shear strengths of various metals which were pressed onto a sapphire substrate. He

found that an increase in the heat of formation of the metal oxide generally results in a decrease in the contact shear strength of the metal oxide interface. This result correlates well with the work of Karnowsky and Estil[39] who found that in the case of direct interfaces, the scratch adhesion strength of metal-ceramic couples increases as the heat of formation of the corresponding metal oxide decreases. Investigations concerning the adhesion of deposited metal films to oxide substrates have therefore lead to the general conclusion that the adhesion which can be attained is inversely proportional to the heat of oxide formation of the deposited material. Many models for the adhesion mechanism have been proposed based on this conclusion. One of the models proposes the formation of a transition region of oxides and sub-oxides of the film and the substrate material at the interface.[40] This requires the diffusion of oxygen through vacuum-evaporated films and gives a time dependence for adhesion which is sometimes observed.[41] Another model requires only that the oxide surface be composed of oxygen ions, as proposed by Weyl [9], with the less polarizable cations being submerged below the surface and screened by the oxygen ions. Bonding then occurs by the direct interaction between the deposited material and the "oxygen" surface. In this model, the time dependence is attributed to the necessity for the film-substrate interface to come to equilibrium. In these models, gold with a bulk free energy

of oxide formation of +39 kcal/mol ( $Au_2O_3$ ), should not adhere to either $Al_2O_3$ or fused silica, commonly used as substrates. Often when depositing gold, an intermediate layer of oxygen-active metal which has solid solubility with gold is used between the gold film and oxide substrate to provide adherence. In thin-film technology, bismuth trioxide is reactively sputtered on an oxide surface to provide nucleation sites and to give better adhesion, electrical and optical properties to the deposited gold film. Apparently, the function of the non-stoichiometric bismuth trioxide is to provide excess bismuth for nucleating the gold film. [42]

Opposed to these models of the adhesion mechanism are the observations of Moore and Thornton on gold melted on a fused silica interface.[10] If the gold is melted on silica with no oxygen present, there is no indication of reaction or adhesion between the gold and silica ; however, if the gold is melted on the surface in the presence of appreciable oxygen there is good adhesion and gold diffuses into the silica surface. The silica surface is extensively etched in the oxide-gold-oxygen interface which also most strongly exhibits the reaction. It has also been demonstrated that the adhesion of a metal to alumina can be enhanced if the metal in contact with the substrate is oxidized. O'Brien and Chaklader[43] found that the work of adhesion between copper and sapphire reached a maximum at an oxygen partial pressure of $10^{-9}$ atmosphere. At an elevated temperature, CuO in

contact with alumina forms a CuAlO spinel intermediate compound at the interface. Katz [44] found out that the measured adhesion of a $Cu/CuO/CuAlO/Al_2O_3$ system is an order of magnitude greater than that of a $Cu/Al_2O_3$ system. This concept was used by Burgess et al [45] to develop the direct copper alumina bonding process for hybrid microelectronic packaging, wherein thick copper films are placed in contact with alumina in a slightly oxidizing atmosphere at just above the eutectic temperature. Under these conditions, a thin molten layer of eutectic forms around the copper and wets the substrate, thus promoting adhesion. Mattox [11] observed that by using the proper conditions it was possible to deposit adherent gold films on fused silica surfaces with no intermediate material. This was done by triode sputtering of gold from a dc cathode and rf sputtering of the silica surface and having oxygen present in the gas discharge. Oxygen has also been used as a "brake" or fixing agent [13] to stop low temperature kinetic processes and has been used successfully to stop agglomeration effects and impede annealing in tin films. In many applications, a need exists for very thin, high purity film specimens that are microscopically smooth. The problem in obtaining high-purity thin films is that as deposition conditions improve agglomeration effects become quite pronounced even at relatively large thicknesses. Thus, to obtain very thin, high purity films which are stable at room temperature, a

technique is required to stop agglomeration. One method is suggested by the work of Keith [46], who performed X-ray diffraction measurements on copper films deposited on liquid oxygen temperature. He found that after deposition, the "nominal grain size" in these films was approximately 40 'A but upon warming to room temperature the grain size increased to at least 400 'A. However, if the film was warmed in a high partial pressure of oxygen, the final grain size was only 60 'A. Caswell and Budo [13] studied the changes in film structure of a thin tin film deposited at low temperatures and then warmed to room temperature. They found that the film starts to agglomerate at a temperature well below room temperature and during later stages of agglomeration, the film consists of isolated islands. Any stage in this metamorphosis was then obtained by annealing the film to the temperature at which the desired micro structure existed and fixing the film with oxygen during further heating of the substrate. Thus, the presence of an oxygen-rich atmosphere was understood to have a stabilizing effect on thin metallic films. Electrical resistance data have been frequently reported in literature to study the effect of oxygen on the agglomeration of thin films like gold and tin.

## 2.4 Thin Film Deposition

There are two types of deposition processes that are useful, namely, chemical vapor deposition and physical vapor deposition.

### 2.4.1. Chemical Vapor Deposition (CVD)

CVD is the growth of thin films using gaseous compounds containing the necessary elements to form the films. The films grown can be amorphous, polycrystalline or crystalline. Metals, semiconductors and insulators have been grown using CVD techniques. The CVD process consists of three steps, i.e.

a) Introduction and equilibrium of the deposition gases into the reactor.

b) Transport of the reactive species to the deposition surface.

c) Nucleation and growth of the thin films.

### 2.4.1 Physical Vapor Deposition (PVD)

There are two types of physical vapor deposition techniques, namely evaporation and sputtering. In both cases, the formation of a deposit on a substrate away from the source consists of three steps, i.e.

a) Converting the condensed phase (generally a solid) into a gaseous or vapor phase.

b) Transporting the gaseous phase from the source to the substrate.

c) Condensing the gaseous phase on the substrate followed by the nucleation and growth of the film.

In both types of deposition, the deposition material is transformed into a gaseous phase where interactions with the residual gases and sputtering gases become important in determining the property of the deposited film.

a) Evaporation Process

Thermal evaporation is the simplest method of depositing thin films. In this method, a film is deposited by the condensation of the vapor on the substrate, which is maintained at a lower temperature than the vapor. All metals vaporize when heated to sufficiently high temperatures. Several methods, such as resistive, induction or radio frequency (RF) , electron bombardment, or laser heating, can be used to attain these temperatures. For transition metals, especially the refractory metals, evaporation using an electron gun is common. For low melting point metals, like aluminum, any of the above methods can be used. Resistive heating is limited in application because of the lower throughput associated with the smaller metal charge generally used in these systems. On the other hand, electron gun evaporations cause radiation damage and, therefore, require a high temperature post-deposition heat treatment to anneal out the radiation damage. The advantage of this method is that the evaporation takes place at considerably

lower pressures than the sputtering pressures, and gas entrapment in the film is almost negligible. RF heating of the evaporating source in an appropriate crucible is probably the best compromise for providing large throughput and a clean environment. Evaporation can also be used to deposit an alloy or a mixture of two or more materials by the use of two or more independently controlled evaporation sources. Experiments are carried out to determine the individual component evaporation rates independently under different conditions. With this information, the condition is chosen to deposit an alloy or a mixture in the desired composition. This method of coevaporation, which has been used to deposit refractory silicides, however, requires good calibration, which must be maintained during a run and from run to run. Coevaporation from a single source containing the alloy constituents is generally not possible, because fractionation occurs as the evaporation proceeds. Fractionation is the phenomenon in which one component evaporates preferentially, leaving the source rich in the other component or components and thus leading to films richer in the preferentially evaporated component.

b) Sputter deposition

Here, the target material is bombarded by energetic ions. Some of the target atoms are thus knocked off the surface, and these atoms are then condensed on the substrate

to form a film. Sputtering processes, unlike evaporation, are very well controlled and are generally applicable to all materials- metals, alloys, semiconductors and insulators. RF, direct current (DC), and DC magnetron sputtering can be used for metal deposition. Alloy film deposition by sputtering from an alloy target is possible because the composition of the film is locked to the composition of the target. The difference in the target and film compositions depends on the type of equipment, the sputtering parameters and the alloy constituents used. By proper choice of the equipment and sputtering parameters, several complex alloys have been deposited with identical compositions in the target and the film. Alloys can also be deposited in a reactive environment. Thus, gases such as methane, ammonia or nitrogen, and diborane can be used in the sputtering chamber to deposit carbide, nitride, and boride, respectively. Sputtering is carried out at relatively higher pressures (0.1 to 1 Pa range). Because gas ions are the bombarding species, the films usually include small amounts of the sputtering gas.[48] These gases in the films are non-reactive except when the sputtering gas is contaminated with chemically active gases. Sputtering is a physical process in which the deposited film is also exposed to ion bombardment. Such ion bombardments cause so-called sputtering damage, which leads to unwanted charges and internal electric fields that affect

device properties. Such damages are generally corrected by annealing at relatively low temperatures, around 500 'C.

## 2.5 Adhesion Tests

For any intended application of a film, its adhesion to the substrate is very important for any practical utilization of the composite. As has been stated by Mittal et al, [49,50] no engineering test is able to measure the basic adhesion. However, a large number of mechanical tests have been proposed to measure the characterize the practical adhesion of thin films, some of which are now reviewed here. There are essentially three type of tests characterized by the kind of stresses they generate in the interfacial region. namely , shear, tensile and scratch tests. The choice of the test should be based upon the type of stresses the test specimen is going to encounter in practice. Additionally , the ideal test should be non-destructive, reproducible, easy to perform and interpret, automated and quantitative.

### 2.5.1 Shear Test

a) Adhesive tape test

This test is essentially qualitative in nature and is used mainly as a quality control for weakly adherent coatings. Semiquantitative results have been obtained if testing conditions such as controlling the pressure while sticking

the tape onto the coating, peeling angle and peeling speed are kept constant. [51] The adhesion is characterized either by the area detached or by the peeling energy.

b) Direct Shear Test

In these methods the force is applied to a glued or soldered element parallel to the surface of the coating [52] or by twisting the element.[53] This method suffers from the limitations of alignment .

c) Peel Test

This test is widely used in the microelectronics industry to measure the adhesion between metallic films and dielectric substrates. However ,the peel strength is a measure of the decohesion energy only under certain conditions which are not generally satisfied when testing practical films. Kim et al, [54,55] have done a detailed analysis of the mechanics of the peel test, where they have shown that the measured peel strength is actually composed of two components : the force required to plastically deform the film , as well as the decohesive force at the interface. They have proposed an universal peel diagram ,for copper films on silicon and polyimide surfaces, from which the interfacial toughness ( decohesive force) can be read directly knowing the peel force and the thickness of the film. This is of

great practical importance since the behavior of films of a range of thickness of 1 to $10^4$ mm is described by this diagram. Nevertheless , this method is still limited by the fact that it can be used only for weakly-adherent coatings.

### 2.5.2 Tensile Test

a) Pull test

In these tests a normal tensile force is applied to the coating to be measured by means of an element glued [56] or soldered [57] to the coating. The characteristic measured value of adhesion is the Stress, F/A. The principal difficulties are related to pulling the element perpendicular to the interface without misalignment.

b) Topple test

This consists of using a different geometry for the glued element , and applying the force necessary to debond the coating parallel to the sample surface. [58] The characteristic measured value is the moment, F x h. These two techniques are limited by the mechanical resistance of the glue, which is for the best glues of the order of 80-90 MPa.

c) Acceleration test

These tests have the advantage of having no mechanical linkage to the test specimen. The tensile stresses are generated by subjecting the film-substrate composite to large acceleration. Two different methods have been described in the literature, the ultracentrifugal and the ultrasonic methods.

i) Ultracentrifugal test

In this test a coated cylinder is levitated electromagnetically and rotated at an increasing speed until the coating debonds from the substrate.[59] The tensile stresses created in the coating are due to the centrifugal forces. The adhesion is given by the relation :

$$\text{Adhesion} = F/A = 4p^2N^2r\rho d - \sigma d/r.$$

where N is the critical number of revolutions per second, r is the cylinder radius, and $\rho$ and d are, respectively, the density and the thickness of the coating. The $\sigma d/r$ term , is the cohesive term, $\sigma$ being the tensile strength of the coating. Both adhesion and cohesion forces have to be overcome in order to detach the coating.

ii) Ultrasonic Test

The principle of this test is to generate ultrasonic vibrations in the sample by means of an electromagnetic or piezoelectric transducer.[60] The adhesion is given by the relation :

Adhesion = F/A = $r_C da$ ,

where $r_C$ is the coating density , $d$ the coating thickness , and $a$ the amplitude of the acceleration when the coating is detached from the substrate.

In both acceleration tests, the tensile stresses generated in the coating in order to detach it from the substrate are directly dependent on the mass, and consequently the thickness of the coating. These tests are suitable for thick film coating of the order of ~ 10 μm . Thin films require extremely large accelerations necessitating costly and sophisticated instrumentation. Furthermore, the maximum adhesion values which can be measured by these tests are only of the order of 10 MPa.[61]

### 2.5.3 Scratch Test

This test proposed by Heavens [62] and then extensively used by Weaver and co-workers, [63,64] employs a step-wise [65,66] or continuously loaded [67,68] spherical scratching point , which is then drawn across the coated sample. The scratching point produces an increasing elastoplastic deformation of the film-substrate system until a damage

occurs in the surface region which can be adhesive or cohesive in nature. The minimum load at which an adhesive failure occurs is called the critical load $L_C$ , and is representative of the coating adhesion. Depending on the film-substrate to be tested , the critical load can be determined by acoustic emission , optical or scanning electron microscopy, and by the variation of the normal, tangential and lateral forces applied to the sample. The main difficulty with the scratch testing technique is to interpret the value of the critical load in terms of adhesion. The critical load depends on several factors, besides adhesion,. These are both intrinsic parameters, depending on the testing conditions ( like scratching speed, loading rate, diamond tip radius and diamond tip wear ) , and extrinsic parameters ( like coating roughness, coefficient of friction and frictional force). These factors make the scratch test results quite difficult to interpret and hence, not very reproducible and quantitative.[69]

The pull-test still remains the easiest to interpret, reproducible and sufficient for the adhesion strengths of interest in the current research , i.e. 0-90 MPa.

# CHAPTER 3

# EXPERIMENTAL

## 3.1 Substrates Used

The ceramic substrates that were investigated for metal-ceramic adhesion were commercially available electronic quality alumina and fused silica. The alumina substrates had an average grain size of 2.5 μm and the surface roughness was ~ 0.1 μm, as measured by a Dektak II surface profilometer. [70] The Alumina was 99.6% pure, and the main impurities were $SiO_2$ and MgO. These substrates were tape-cast by Coors Ceramic Company. The fused Silica substrates were high purity synthetic materials manufactured by the flame hydrolysis of $SiCl_4$. They were amorphous and the polished samples had an average surface roughness of ~ 20°A. The total trace impurities were less than 0.2 ppm. They were manufactured by a process that reduced OH content and improved index homogeneity. They were obtained from Heraeus Amersil Inc. under the trade name, Suprasil 2.

## 3.2 Laser Irradiation

The laser irradiations were performed in the Solid State Division of ORNL, with a pulsed XeCl excimer laser (308 nm wavelength). A schematic of the laser equipment setup is illustrated in Figure 3.1.The substrates to be irradiated were

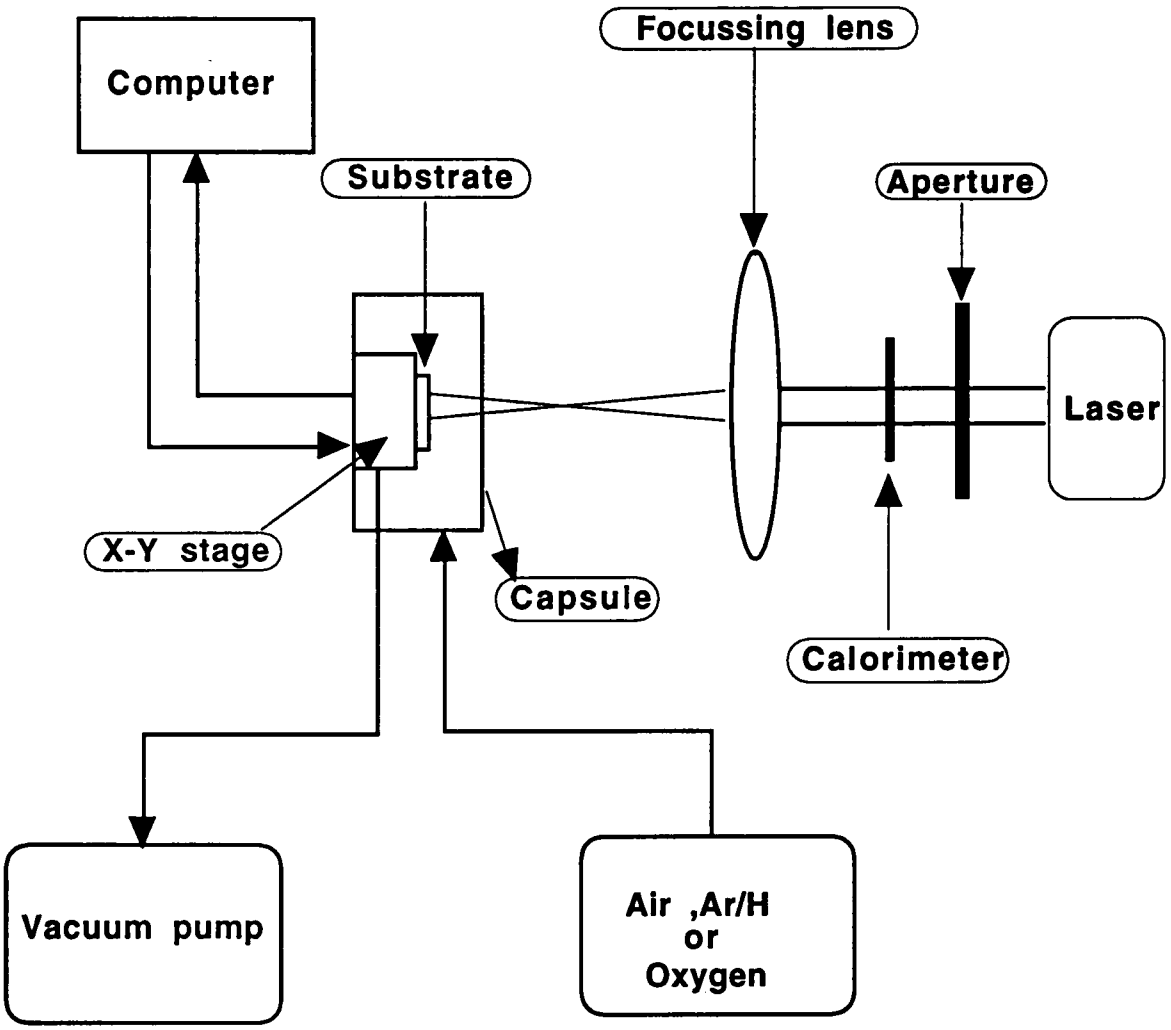


Fig.3.1 Schematic of the laser equipment setup.

placed on a computer controlled X-Y stage. The X-Y stage could be moved with a resolution of 1μm and the substrates were held onto them by vacuum. The output laser energy was measured by an energy calorimeter and was about 300-600 mJ. The actual energy density on the sample surface could be varied between 0.1 and 10 $J/cm^2$ by varying the distance between the focusing lens and the sample. The pulse duration of the laser was ~41 ns and the pulse repetition rate was 0.3 Hz. The samples could be laser irradiated either in air, reducing, oxidizing or inert atmospheres by using a gas capsule to enclose the specimen.

### 3.3 Thin Film Deposition

Thin film depositions were performed using ion beam deposition in the Gatan Dual Ion Mill. The depositions were carried out under the following conditions : gun voltage = 10KV, gun current = 1 mA , and gun tilt = 30°. The base pressure during pumpdown was less than $5X10^{-5}$ torr. Argon was used as the ionizing gas medium for the depositions. During deposition the chamber pressure was around $1X\ 10^{-4}$ torr. The deposited film thickness for thin film adhesion tests was 800 °A. The deposition rates of gold and nickel films were calibrated by depositing them on a clean piece of glass for different times under the above conditions of gun voltage, current and tilt. The film thickness obtained was then calibrated using a Dektak profilometer. Ion beam sputter deposition gave gold film thickness of 800 °A in 2 minutes and

nickel film thickness of 800°A in 4 minutes under the above conditions.

### 3.4 Pull Testing

The adhesion strength of the metal-ceramic couples was measured by an indegeneously developed pull-testing apparatus as shown in Figure 3.2. Epoxy coated Aluminum pins with a pin-head diameter of 0.106 inches were used. The strength rating of the epoxy was ~ 80 MPa. The pins were placed on the metal-ceramic couples with an elastic clamp, and the whole assembly was placed in a furnace to cure the epoxy. The curing was done at 150 °C for 90 minutes and then the furnace was allowed to cool down slowly. Perfect alignment of the pin in the pulling direction was ensured to eliminate any shear stresses. The load was applied by a stepper motor which pulled down at a rate of 3 μm / sec. This was monitored by a Step-pak controller which was in turn allowed to interface with a computer. The load was measured by a peizo-electric transducer which also communicated data to the computer. The sensitivity of the transducer was 0.01 lb. After failure, pin and substrate were examined both visually and by using an optical microscope to establish whether the film had failed at the metal-ceramic interface or in the glue. Usually, failure occurred in the glue if no metal film was detected around the pin edges, or if the metal-

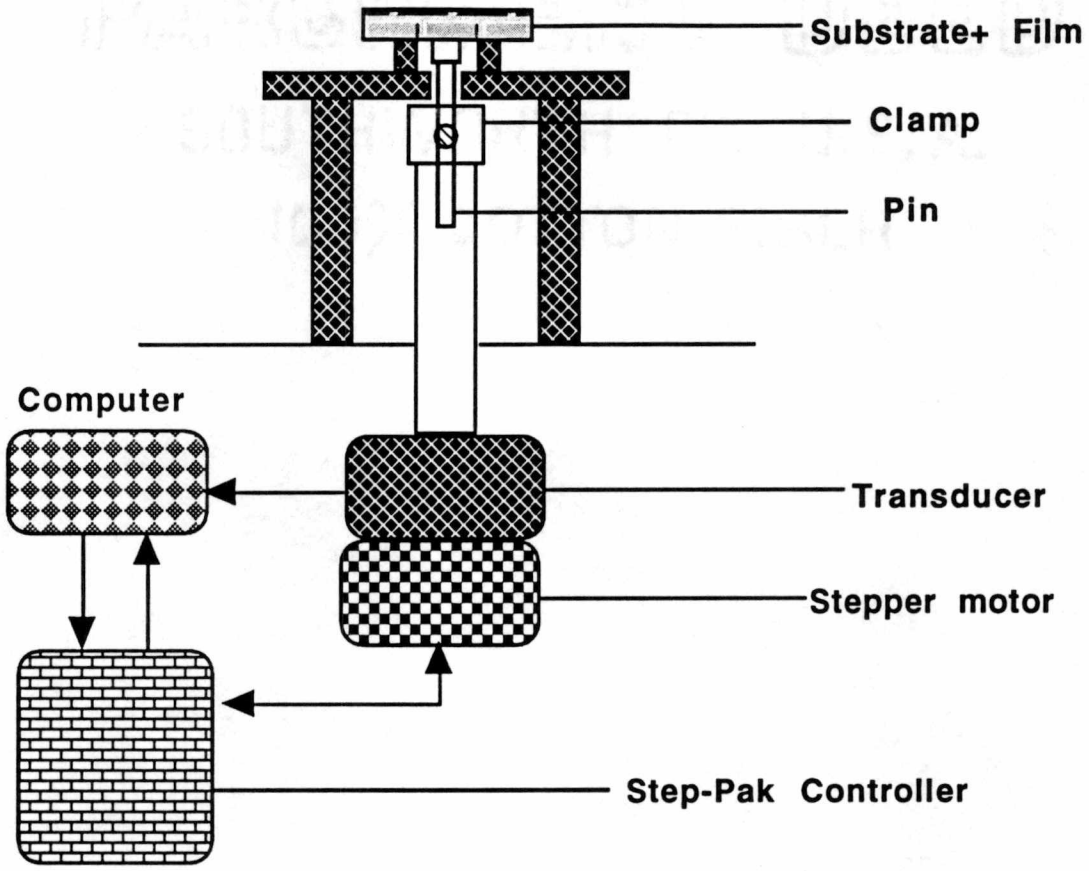


Fig. 3.2. Schematic of the pull-testing apparatus.

ceramic couple failed at a very high load, or if there was considerable plastic flow before failure.

## 3.5 Annealing Treatments

These were performed in a tube furnace and were either carried out in a reducing atmosphere or under vacuum. The vacuum was achieved by connecting the furnace to a diffusion pump backed by a roughing pump as shown in Fig. 3.3. When the annealing was done in a reducing atmosphere, the furnace was evacuated to a certain pressure, i.e. 20 mbar and then flushed with $Ar/H_2$ . This evacuation and flushing was repeated four times to ensure a completely reducing atmosphere in the furnace. The pressure inside the furnace was measured using a pirani gage for pressures up to 1 mbar and a penning gage for pressures in the range of $10^{-3}$ - $10^{-6}$ bar. The furnace chamber was first heated up to the desired annealing temperature using a controller which interfaced with a computer. The sample was then introduced into the chamber with the help of an external magnet as shown. After annealing for the required time, the sample was withdrawn from the chamber using the magnet.

## 3.6 In-situ Resistivity Measurements

The resistance changes of some of the metal-ceramic couples were studied as they were heated up from room

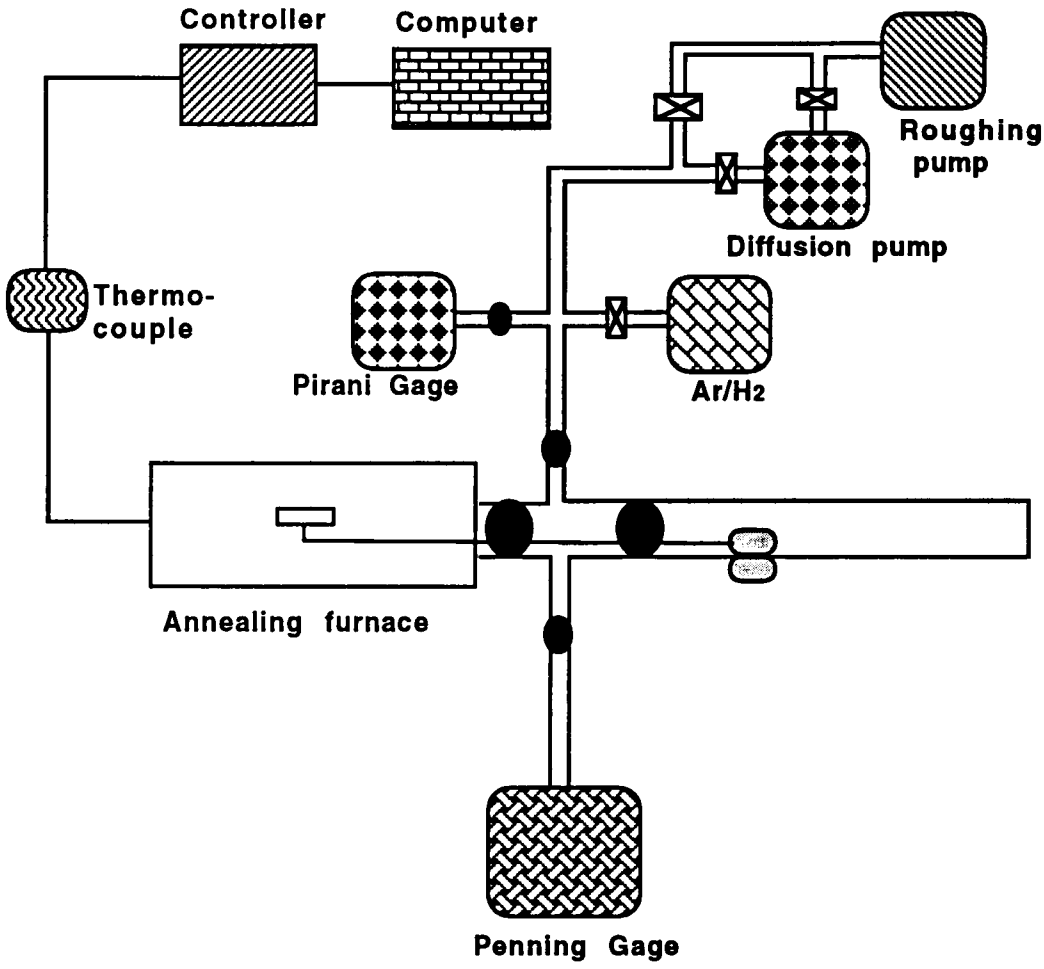


Fig. 3.3. Schematic of the set-up of the annealing of metal-ceramic couples.

temperature in the tube furnace. Two samples processed under different conditions were studied simultaneously to compare and contrast the effects of different types of laser treatment. A suitable mask was used to prepare such a sample as shown in Fig.3.4. The resistance changes were recorded in an Auto-ranging Keithley 193, multimeter. The data was then transferred to the computer using an IEEE-interface. A thermocouple was also introduced near the sample to record the sample temperature and this also interfaced with the computer, thus recording data automatically.

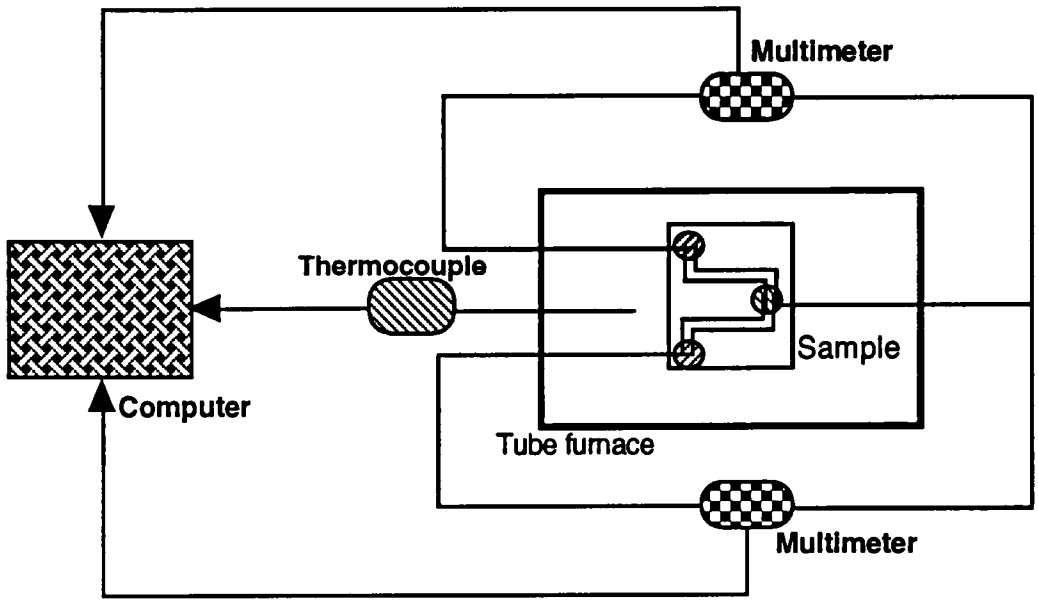


Fig. 3.4. Schematic of the in-situ resistance experiment.

# CHAPTER 4

# RESULTS

## 4.1 Adhesion Testing

Laser treatment of the alumina and fused silica specimens was done at different energy densities in three different atmospheres, e.g. $Ar/H_2$, air and oxygen. Following laser treatment, 80 nm thick metal films of gold, nickel or copper were ion-beam sputter deposited using 10 kV $Ar^+$ ions and an Ar pressure of $5 \times 10^{-5}$ Torr with the base pressure being $< 1 \times 10^{-6}$ Torr. One half-set of the samples was then annealed at 300 °C for one hour. Both sets were then subject to the pull-test to determine the adhesion strength of the metal-ceramic couples.

### 4.1.1 Alumina-Gold

The adhesion strength of as-received alumina-gold samples was very poor (~0.1 MPa). The 300 °C annealing treatment performed after deposition had no effect on unirradiated alumina-gold couples. In fact, the adhesion was so weak that these samples were very difficult to handle without breaking the film. When the samples were laser irradiated in Ar-4%$H_2$ (reducing) atmosphere, the adhesion strength increased to about 1 MPa at 1 J/cm$^2$. The adhesion strength showed a maximum of about 1.2 MPa at 1.5 J/cm$^2$ as

shown in Fig. 4.1. The post-deposition annealing treatment at 300 °C further improved the adhesion strength to 3 MPa for substrates laser irradiated at 1.5 $J/cm^2$ in the reducing ambient, about 30 times better than the as-received samples.

However, increasing the oxygen content of the laser-irradiation ambient produced an even more striking improvement in the adhesion strength. Figure 4.2 shows the adhesion strength of alumina-gold couples as a function of laser energy density for samples irradiated in air. It was observed that without any post-annealing, the adhesion strength reached a maximum of ~ 15 MPa at a laser $E_d$ slightly greater than 1 $J/cm^2$ , about 150 times better than unirradiated substrates. The post-deposition annealing virtually doubled the maximum adhesion strength to ~ 30 MPa, for samples irradiated with an $E_d$~ 1 $J/cm^2$ in air.

When laser treatment was carried out in a pure oxygen atmosphere, the adhesion strength showed further improvement, as shown in Figure 4.3. The maximum in this case was ~ 27 MPA for a laser $E_d$ ~ 1 $J/cm^2$ without any post-annealing. Finally, the post-deposition annealing of samples laser treated in oxygen, showed a maximum adhesion strength of ~ 50 MPa at $E_d$ ~ 1 $J/cm^2$. Thus, starting with an adhesion strength of ~0.1 MPa for films deposited on unirradiated alumina substrates, an increase to ~ 50 MPa for the films deposited on substrates that were laser-irradiated in oxygen at 1 $J/cm^2$ and annealed at 300 °C was obtained for gold-alumina couples.

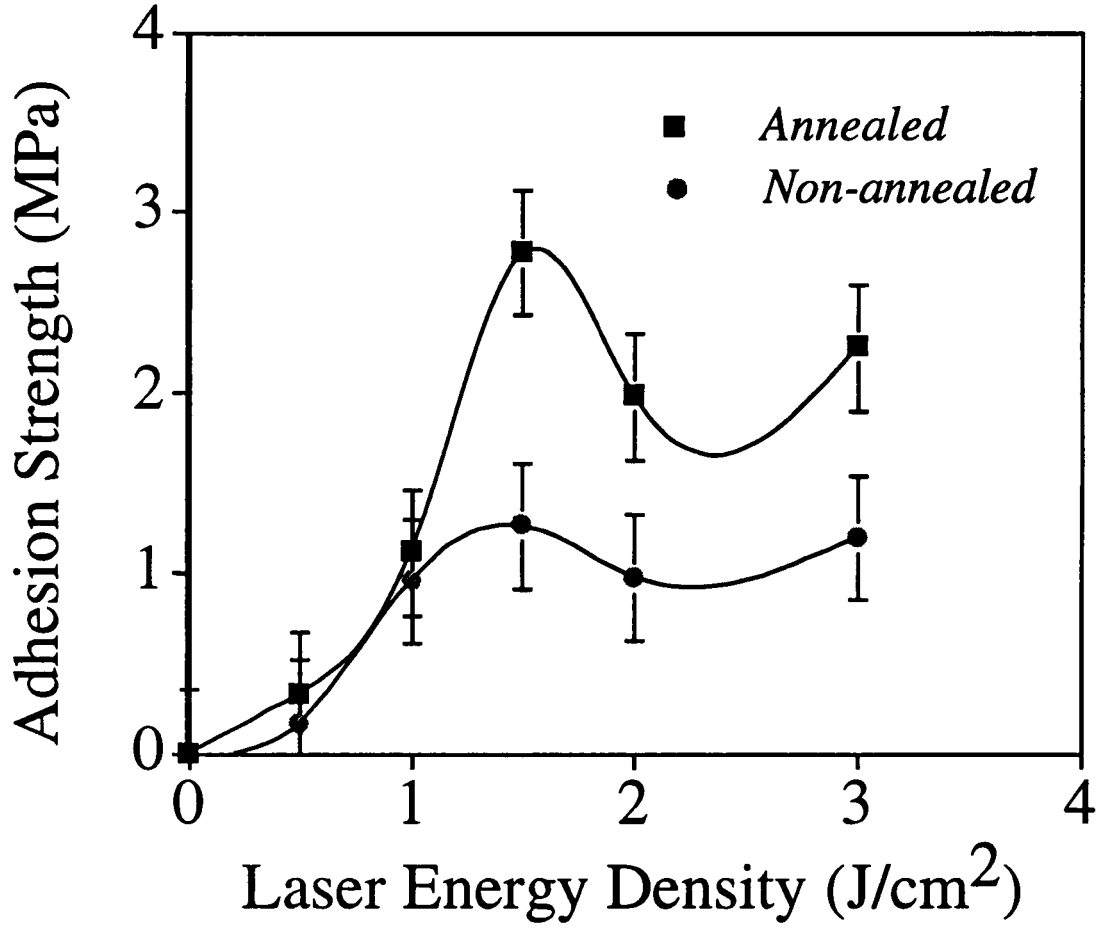


Figure 4.1. Adhesion strength of gold-alumina couples as a function of laser energy density. The alumina substrates were laser treated in $Ar/H_2$.

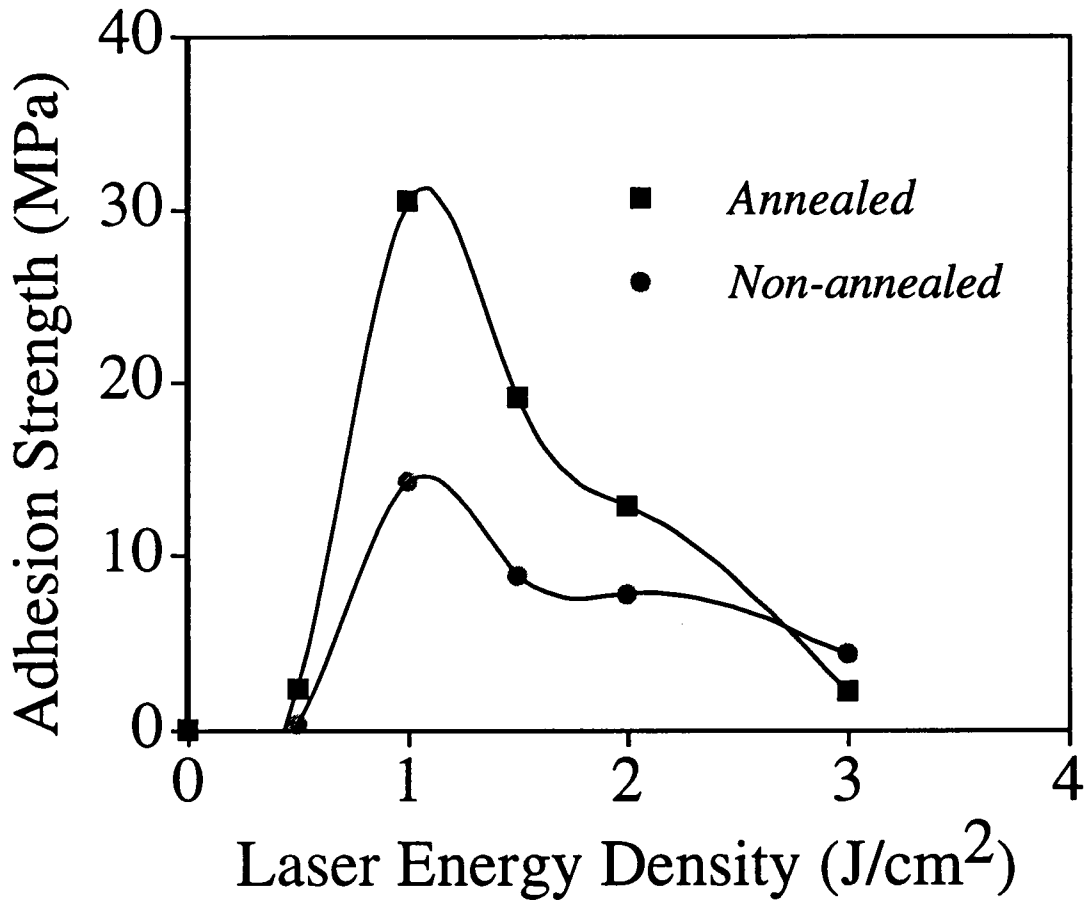


Figure 4.2. Adhesion strength of gold-alumina couples as a function of laser energy density. The alumina substrates were laser treated in air.

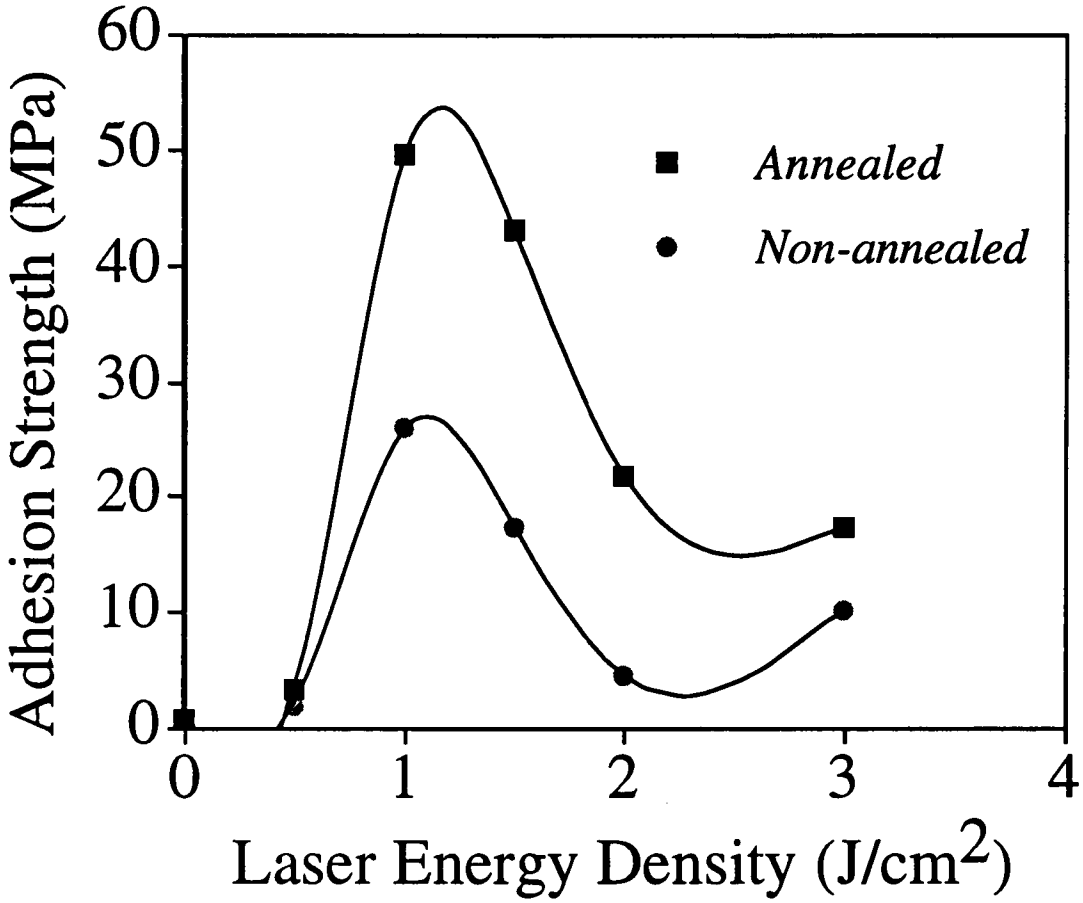


Figure 4.3. Adhesion strength of gold-alumina couples as a function of laser energy density. The alumina substrates were laser treated in oxygen.

Figures 4.4 and 4.5 summarizes the results of the adhesion strengths obtained as a function of laser treatment at three different atmospheres both for post-deposition annealed as well as non-annealed samples.

### 4.1.2 Alumina-Nickel

The adhesion strength of as-received alumina-nickel couple was quite high as compared to that of alumina-gold. The adhesion strength observed for unirradiated samples was ~28 MPa. Laser treatment in $Ar/H_2$ improved the adhesion strength to a maximum of ~57 MPa at a laser $E_d$ ~ 1 J/cm$^2$ as shown in Fig. 4.6, while laser treatment in air improved the adhesion to a maximum of ~ 63 MPa at the same energy density, as shown in Fig. 4.7. A 300 °C post-deposition annealing doubled the adhesion strength of unirradiated samples to ~ 55 MPa. Pull test results of samples irradiated at an $E_d$ > 1 J/cm$^2$ whether in air or in $Ar/H_2$ did not fail at the metal-ceramic interface but instead failed in the glue. Thus, these samples had an interfacial strength greater than that of the glue (> 78 MPa).

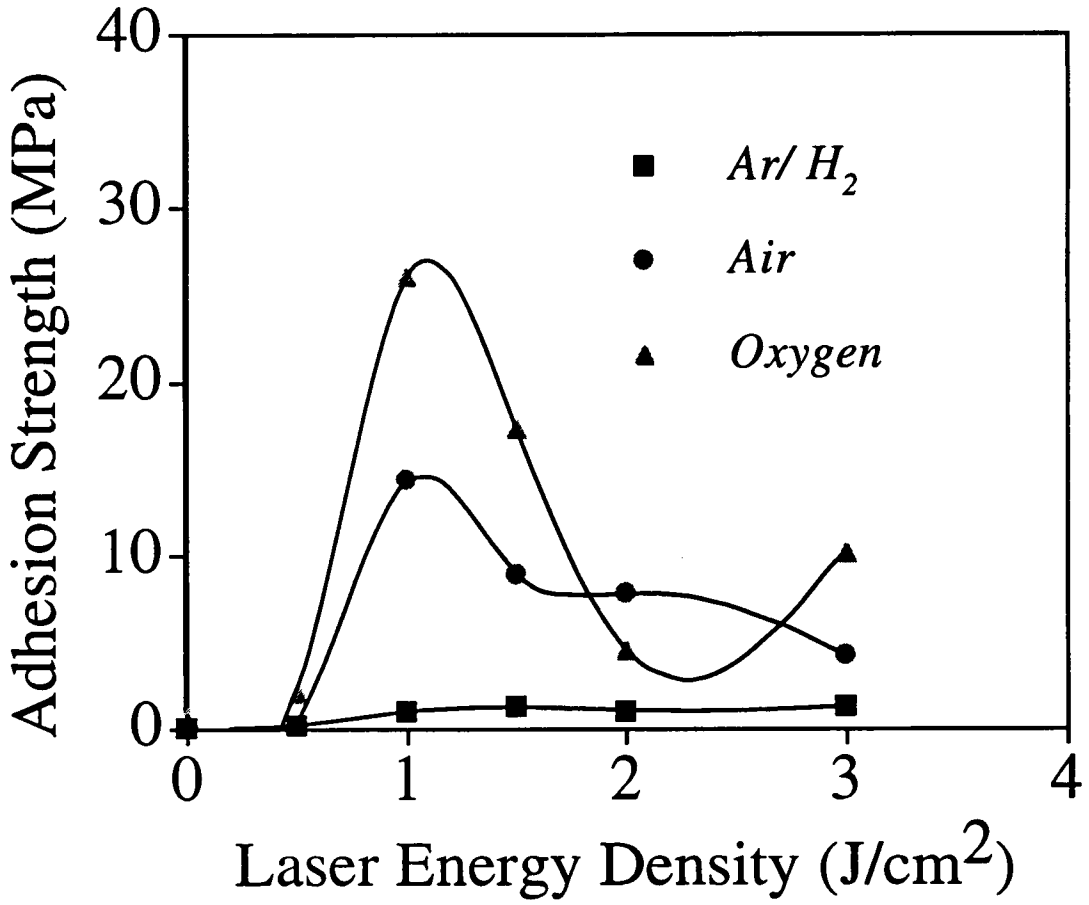


Figure 4.4. Adhesion strength of gold-alumina couples as a function of laser energy density. The alumina substrates were laser treated in three different atmospheres.

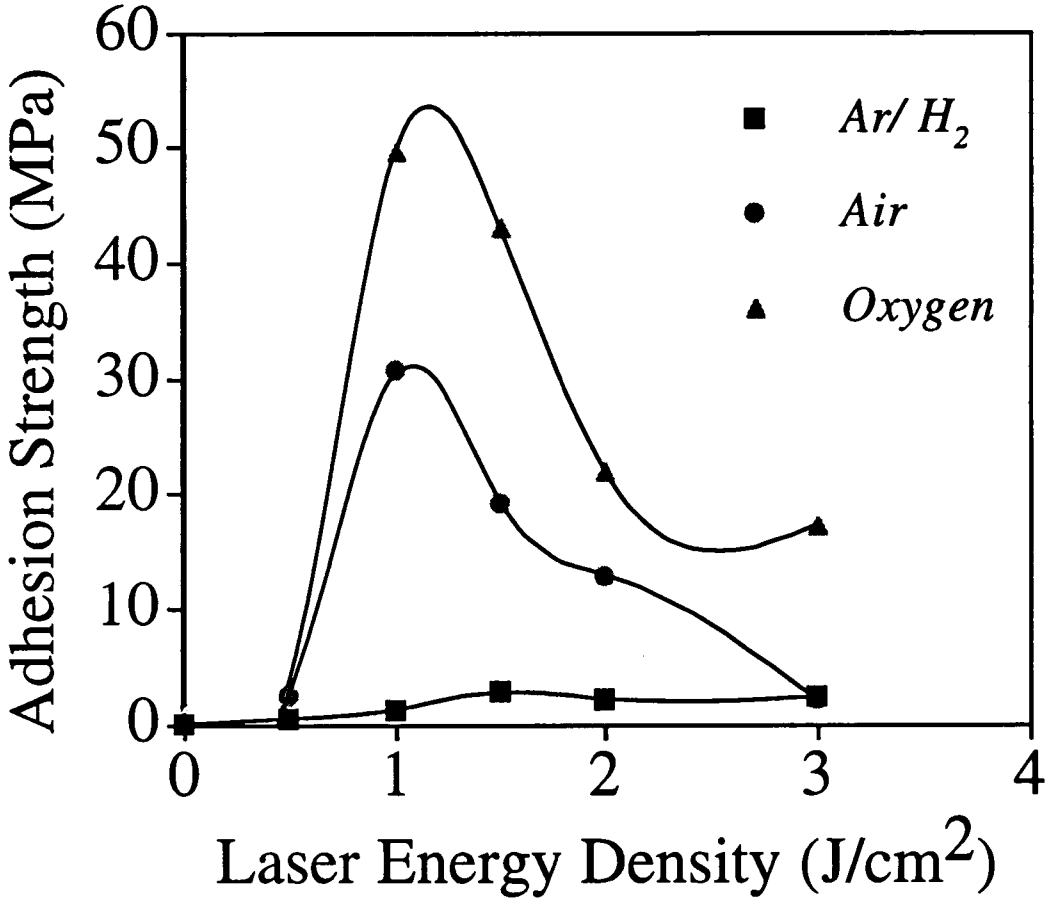


Figure 4.5. Adhesion strength of gold-alumina couples as a function of laser energy density. The alumina substrates were laser treated in three different atmospheres and the couples were subjected to a 300 ° C post-deposition annealing.

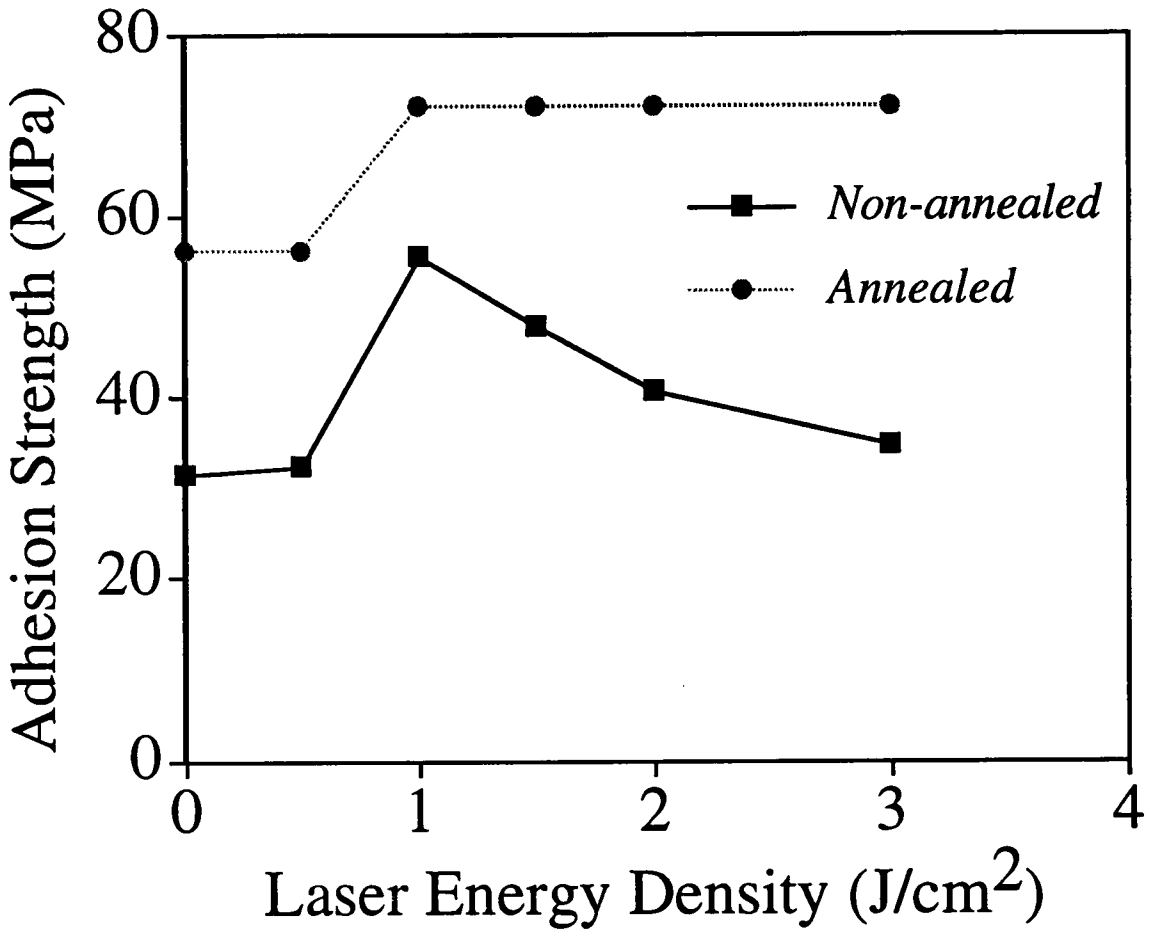


Figure 4.6. Adhesion strength of nickel-alumina couples as a function of laser energy density. The alumina substrates were laser treated in $Ar/H_2$.

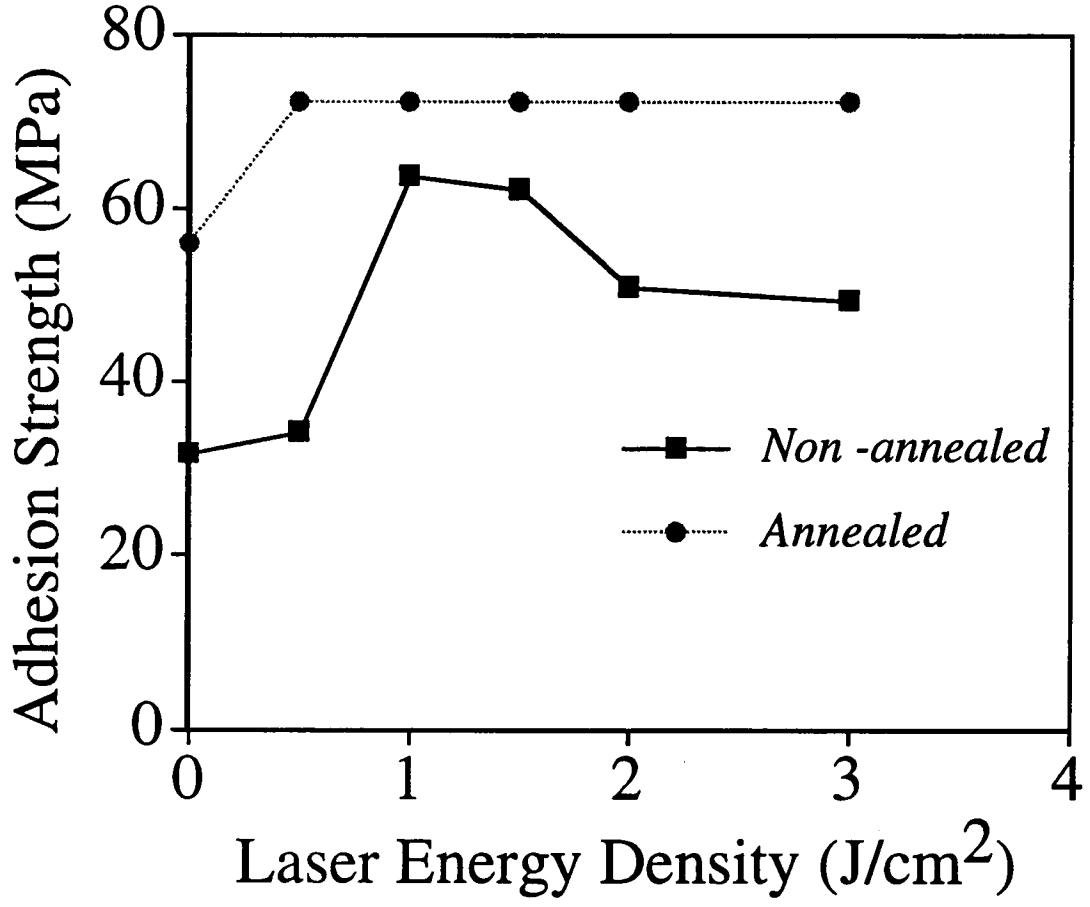


Figure 4.7. Adhesion strength of nickel-alumina couples as a function of laser energy density. The alumina substrates were laser treated in air.

### 4.1.3 Silica-Gold

The adhesion strength of as received silica-gold couples was very poor. The 300 °C annealing treatment performed after deposition had no effect on unirradiated samples. When the substrates were laser irradiated in Ar-4%$H_2$ , the adhesion strength improved to only ~ 1 MPa at 2 J/$cm^2$. Increasing the oxygen content of the laser treating ambient by laser treating in air or in pure oxygen, did not seem to have any profound effect on the adhesion strength of gold-silica couples. A maximum of 1.8 MPa adhesion strength was obtained for a fused silica substrate laser treated in oxygen at 2 J/$cm^2$. The post-deposition annealing treatment only marginally improved this adhesion strength to ~ 4 MPa for laser treatment in oxygen at 2 J/$cm^2$ , as shown in Fig. 4.8.

### 4.1.4 Silica-Copper

Silica-Copper couples also showed very poor adhesion strength. Also, neither the oxygen content of the laser treating ambient nor the post-deposition annealing seemed to have the same effect as was observed in the case of gold-alumina couples. A maximum adhesion strength of only 3 MPa was obtained. This was for a fused silica substrate laser treated in oxygen at 1 J/$cm^2$ , following which an 80 nm copper film was deposited on the fused silica substrate and then the silica-copper couple was subjected to a 300 °C anneal.

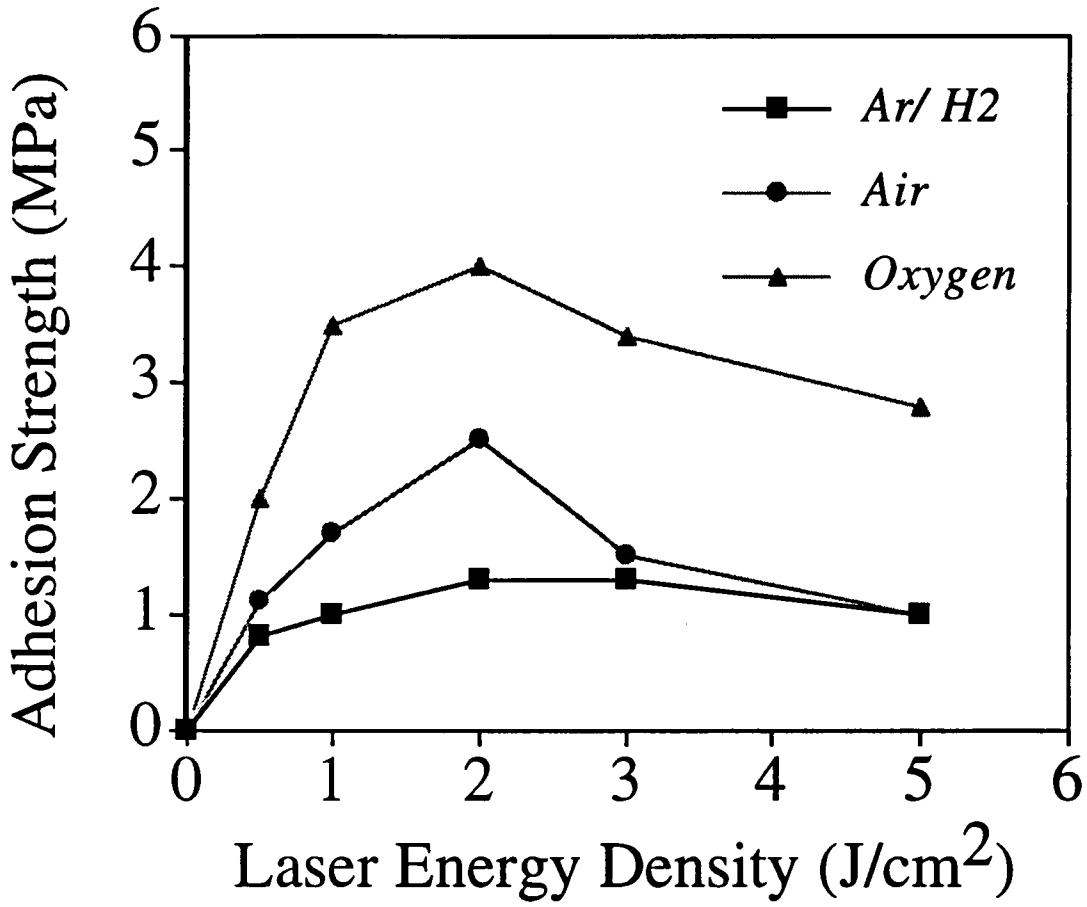


Figure 4.8. Adhesion strength of gold-silica couples as a function of laser energy density. The silica substrates were laser treated in three different atmospheres and the couples were subjected to a 300 ° C post-deposition annealing.

## 4.2. Electrical Resistance Measurements

Resistance measurements were carried out for alumina-gold couples. Alumina samples were laser treated in three different atmospheres, $Ar/H_2$, air and oxygen at different energy densities. Thin gold films of 20 nm thickness were then ion-beam sputter deposited using 6 KeV $Ar^+$ ions. The samples were then annealed at 550 °C for 45 minutes. A two-probe resistivity test was performed afterwards at room temperature. The resistance values of the different samples are presented in Table 4.1. Weakly adherent coatings show a resistance value in the kilo-ohm and mega-ohm range, while strongly adherent coatings show resistance values of the order of only tens of ohms.

Figures 4.9-4.11 show a joint plot of the pull-test adhesion results with the two-probe resistance results. It can be seen that the adhesion strength and the resistance vary in opposite sense with laser energy density for all of the irradiation atmospheres, e.g. $Ar/H_2$ , air and oxygen. The adhesion strength has a maximum value at a laser energy density of ~ 1 $J/cm^2$ for all the three laser irradiation atmospheres, while the resistance curves show a minimum value at the same energy density. These plots, thus, establish the inverse relationship between adhesion strength and resistance.

Table 4.1. Resistance (in KΩ) of a 20-nm thick gold film ion-beam sputter deposited onto an alumina substrate and then subject to a post-deposition annealing at 550 °C for 45 minutes.

| Laser $E_d$ (J/cm$^2$) | $Ar/H_2$ (KΩ) | Air(KΩ) | Oxygen(KΩ) |
|---|---|---|---|
| 0 | 15600 | 15600 | 15600 |
| 0.5 | 9500 | 1680 | 0.876 |
| 1 | 0.431 | 0.296 | 0.088 |
| 2 | 900 | 1.16 | 0.937 |
| 3 | 2520 | 600 | 7.1 |

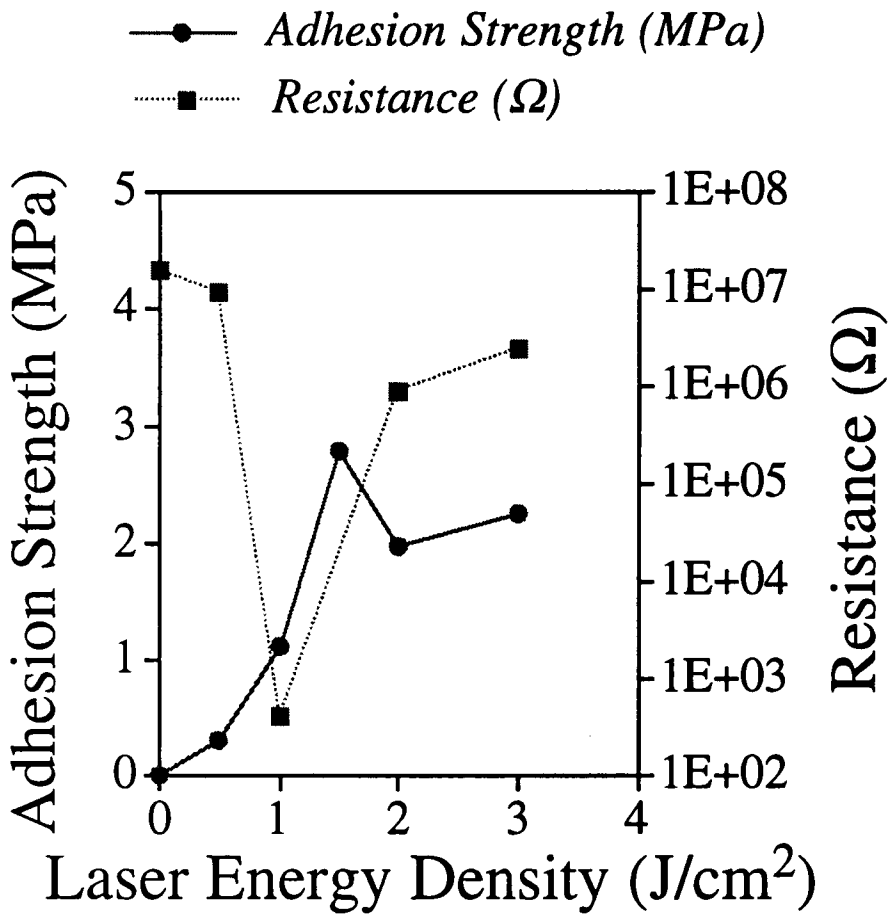


Figure 4.9. Adhesion strength and resistance as a function of laser energy density. The laser irradiations were carried out in a reducing atmosphere, i.e. $Ar/H_2$.

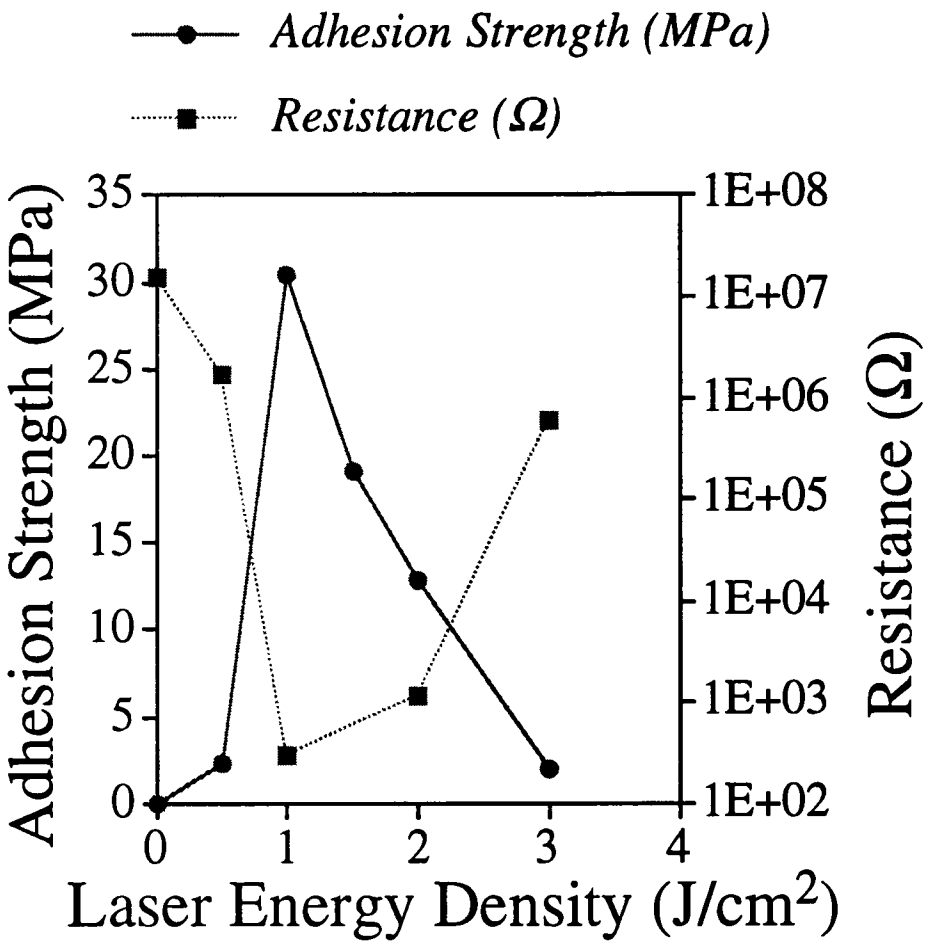


Figure 4.10. Adhesion strength and resistance as a function of laser energy density. The laser irradiations were carried out in air.

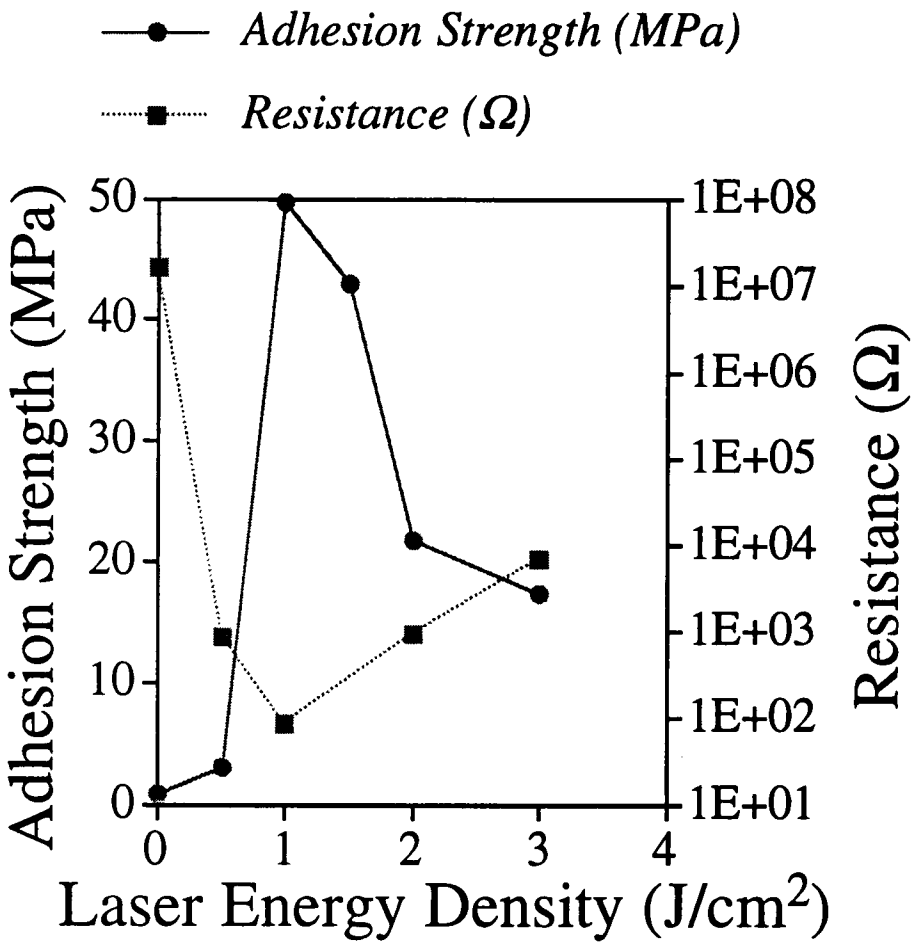


Figure 4.11. Adhesion strength and resistance as a function of laser energy density. The laser irradiations were carried out in oxygen.

## 4.3 Scanning Electron Micro graphs

Alumina substrates were laser treated in three different atmospheres, $Ar/H_2$, air and oxygen at different energy densities. Thin gold films of 20 nm thickness were ion-beam sputter deposited on these substrates using 6 KeV $Ar^+$ ions. The couples were then annealed at 550 °C for 45 minutes. Surface observations were conducted in an S-120 Hitachi SEM. Figures 4.12-4.14 show respectively substrates laser treated in $Ar/H_2$ , air and oxygen, all of them at 2 $J/cm^2$. The film deposited on the substrate laser treated in $Ar/H_2$ shows complete breakdown into small islands and formation of local agglomerates throughout. The film deposited on the substrate laser treated in air shows much less breakdown and agglomeration. The film deposited on the substrate laser treated in oxygen is almost continuous showing even less breakdown and almost no agglomeration. Figs.4.15-4.19 show films deposited on substrates respectively- as-received and laser treated in air at 0.5, 1, 2 and 3 $J/cm^2$. It is found that films deposited on as-received substrates break down completely into small islands. At 0.5,2 and 3 $J/cm^2$ the islands are fewer in number and larger in size indicating that the film breakdown is retarded after laser treatment. At 1 $J/cm^2$ , the film is almost complete, showing very little breakdown. Finally, Figure 4.20 shows a film deposited on a substrate laser treated in oxygen and then subject to

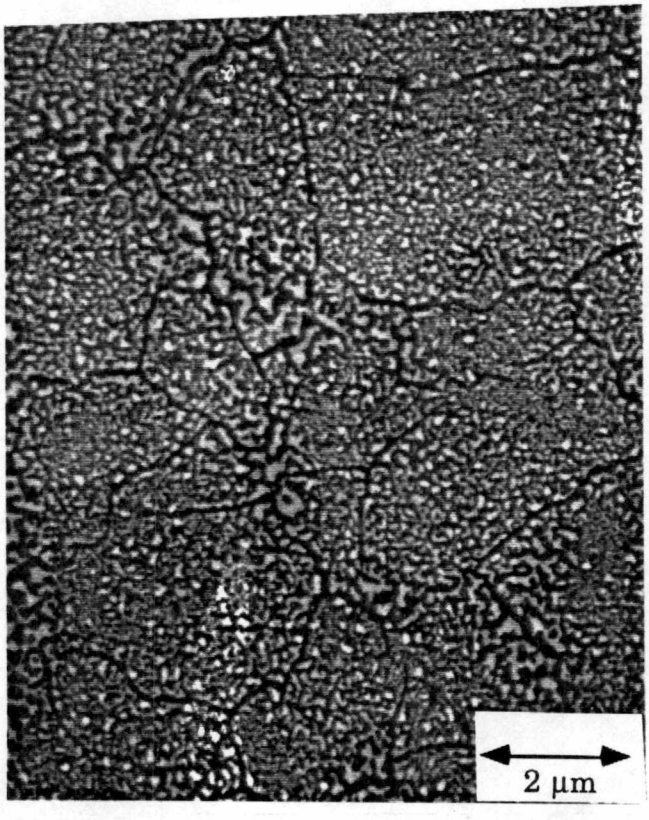


Figure 4.12. SEM micro graph of a 20-nm thick gold film sputter deposited on an alumina substrate laser treated in $Ar/H_2$ at 2 $J/cm^2$ and then subjected to a 550 °C post-deposition annealing for 45 minutes.

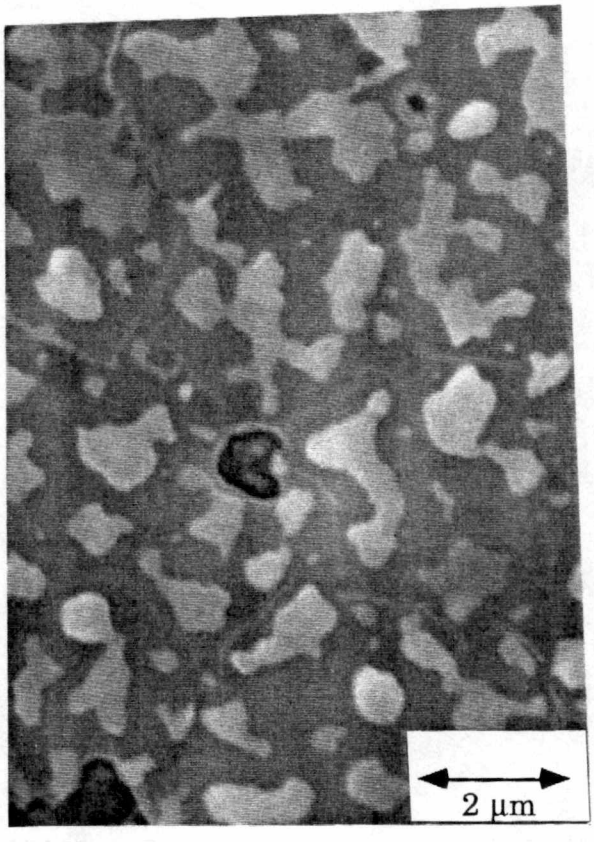


Figure 4.13. SEM micro graph of a 20-nm thick gold film sputter deposited on an alumina substrate laser treated in air at 2 J/cm$^2$ and then subjected to a 550 °C post-deposition annealing for 45 minutes.

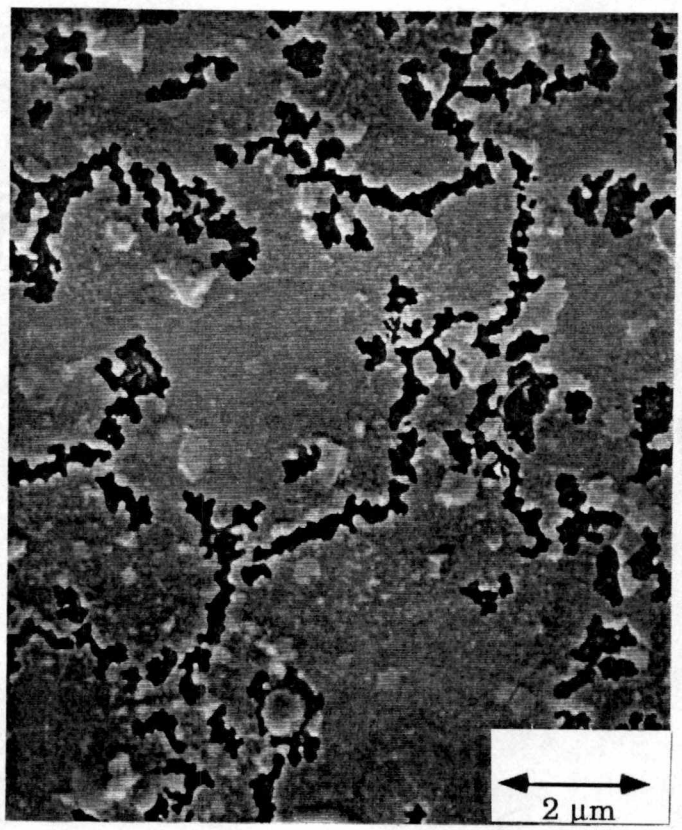


Figure 4.14. SEM micro graph of a 20-nm thick gold film sputter deposited on an alumina substrate laser treated in oxygen at 2 J/cm$^2$ and then subjected to a 550 °C post-deposition annealing for 45 minutes.

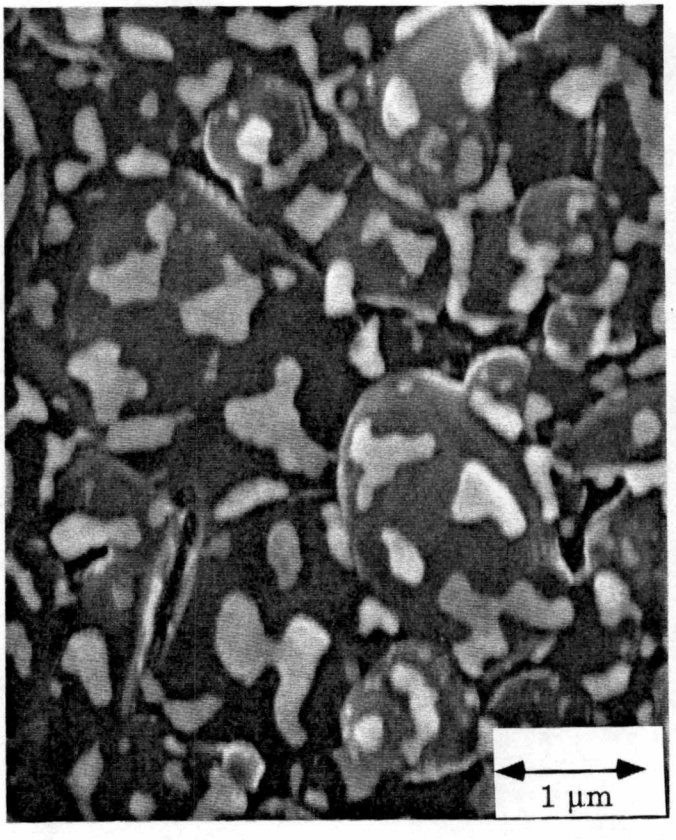


Figure 4.15. SEM micro graph of a 20-nm thick gold film sputter deposited on an as-received alumina substrate and then subjected to a 550 °C post-deposition annealing for 45 minutes.

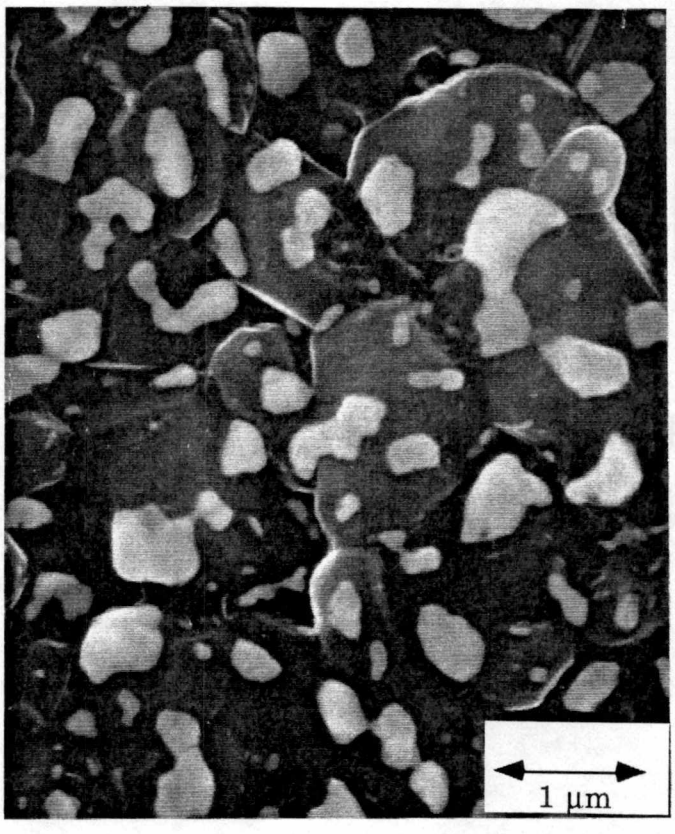


Figure 4.16. SEM micro graph of a 20-nm thick gold film sputter deposited on an alumina substrate laser treated in air at 0.5 J/cm$^2$ and then subjected to a 550 °C post-deposition annealing for 45 minutes.

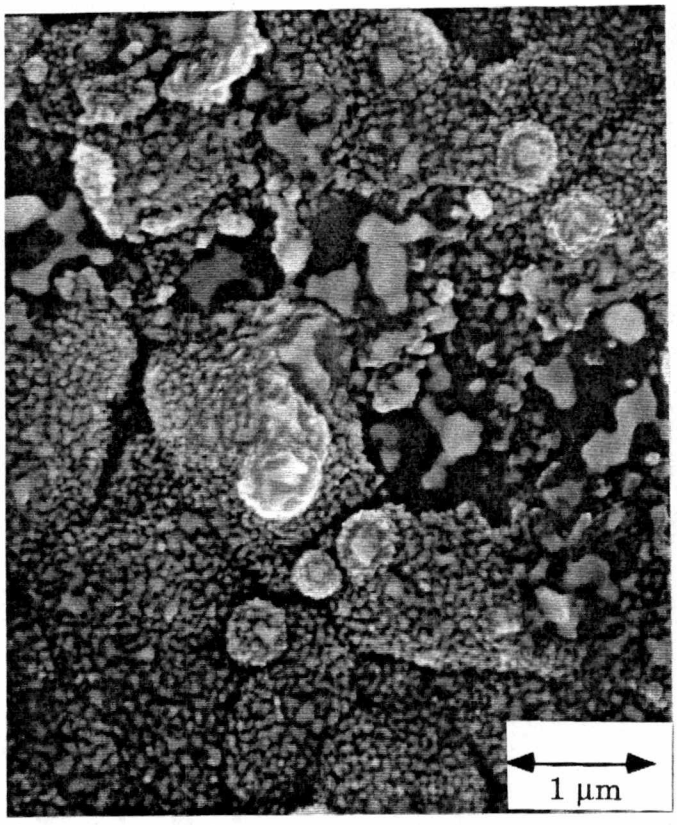


Figure 4.17. SEM micro graph of a 20-nm thick gold film sputter deposited on an alumina substrate laser treated in air at 1 J/cm$^2$ and then subjected to a 550 °C post-deposition annealing for 45 minutes.

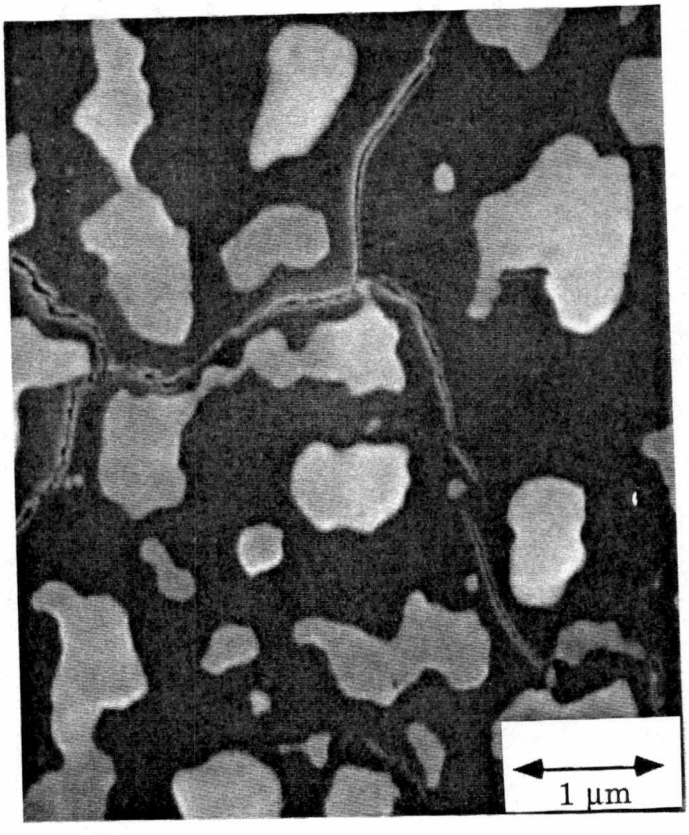


Figure 4.18. SEM micro graph of a 20-nm thick gold film sputter deposited on an alumina substrate laser treated in air at 2 J/cm$^2$ and then subjected to a 550 °C post-deposition annealing for 45 minutes.

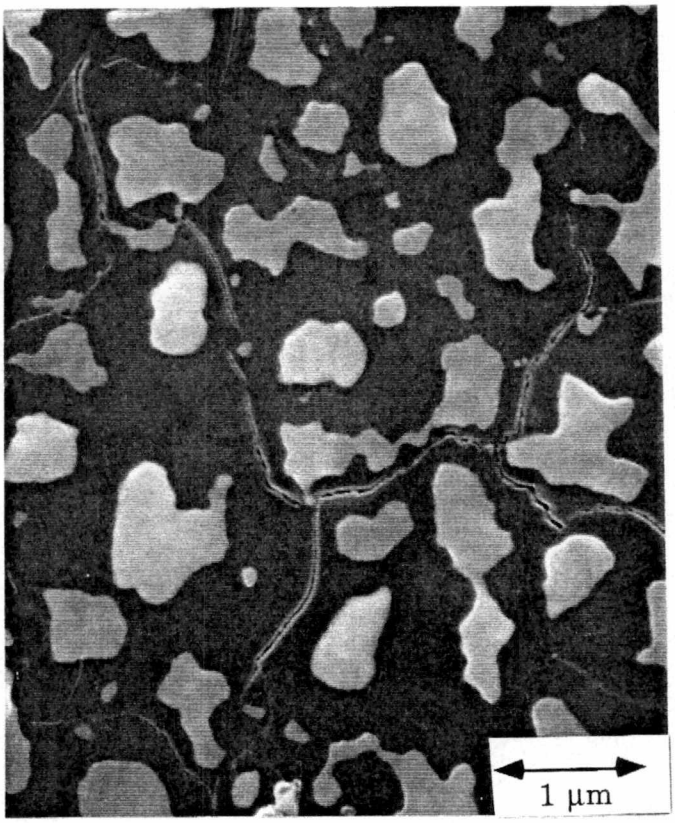


Figure 4.19. SEM micro graph of a 20-nm thick gold film sputter deposited on an alumina substrate laser treated in air at 3 J/cm$^2$ and then subjected to a 550 °C post-deposition annealing for 45 minutes.

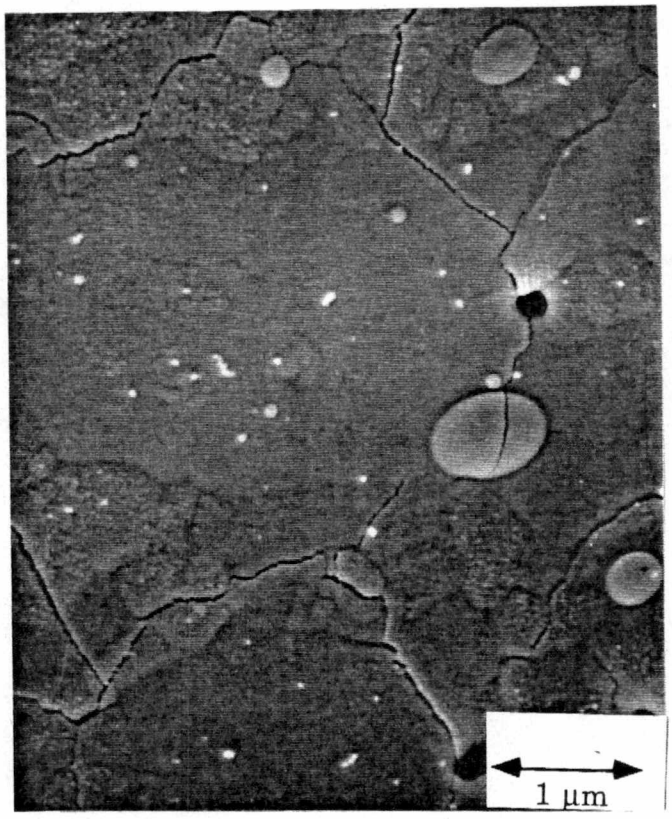


Figure 4.20. SEM micro graph of a 20-nm thick gold film sputter deposited on an alumina substrate laser treated in oxygen at 1 J/cm$^2$ and then subjected to a 550 °C post-deposition annealing for 45 minutes.

annealing at 550 °C for 45 minutes. The film here is complete and shows no signs of breakdown.

## 4.4. In-situ Resistivity Measurements

Two samples, processed under different conditions were annealed simultaneously in the tubular furnace using the arrangement shown in Figure 3.4. Resistance measurements were made in-situ and plotted as a function of annealing time. Figure 4.21 shows the resistance changes of a 200 A° gold film deposited on an as-received substrate and of a similar film deposited on a substrate that was laser treated in oxygen at 1 $J/cm^2$ . Both these substrates were then annealed at 600 °C. It was found that the film deposited on the as-received substrate began to break down into islands in a shorter time than the film deposited on the laser treated substrate. Figure 4.22 shows the resistance changes in a 600 °A gold film deposited on a substrate laser treated in oxygen at 1 $J/cm^2$ and on a substrate laser treated in oxygen at 3 $J/cm^2$ and then annealed at 650 °C. It was found that the film deposited on the substrate laser treated in oxygen at 3 $J/cm^2$ began to break down into islands in a shorter time than the film deposited on the substrate laser treated in oxygen at 1$J/cm^2$ .

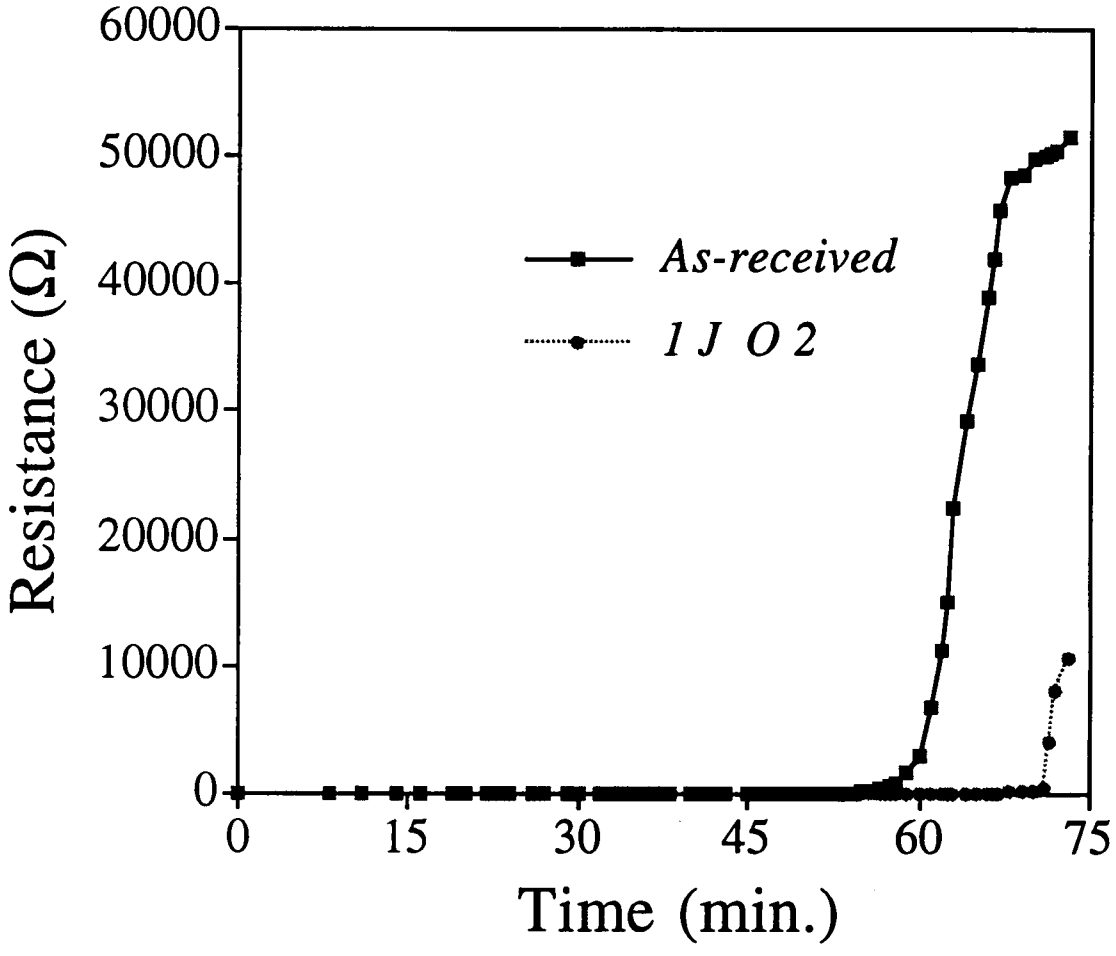


Figure 4.21. Resistance changes in a 200 A° gold film deposited on as-received alumina and alumina laser treated in oxygen at 1 J/cm$^2$ .

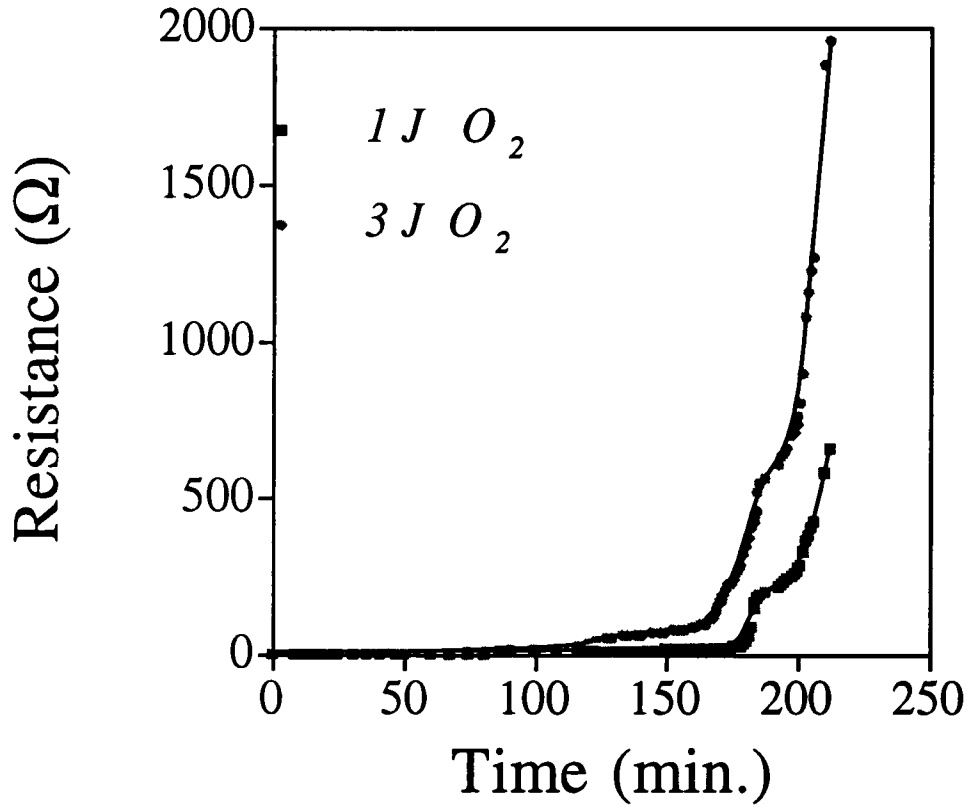


Figure 4.22. Resistance changes in a 600 A° gold film deposited on alumina laser treated in oxygen at 1 J/cm$^2$ and 3 J/cm$^2$ .

# CHAPTER 5

# DISCUSSIONS

## 5.1. Laser Enhanced Adhesion

Laser irradiation of alumina using pulsed XeCl laser causes melting and ablation of the alumina surface. The melting threshold is ~ 0.7 J/cm$^2$. [6] The energy of the incident laser pulse is transferred to the lattice in a very short time, ~ $10^{-12}$ to $10^{-11}$ s, while the pulse duration is 41 ns and the melted region resolidifies in ~200 ns.[5] Hence, two essential features of the excimer laser-solid interaction become important. Firstly, the short time in which energy is transferred to the lattice means that the heating and quenching cycles have a short duration as well and, hence thermally activated processes in the solid state, like diffusion and phase transformations are highly inhibited or almost suppressed. Secondly, the longer duration of the laser pulse compared to the time taken to transfer energy to the crystal indicates some sort of chemical bonding. The rapid melting and solidification and the volume change associated with it produces a lot of defects in the substrate, vacancies and interstitials. These defects provide a means for attachment for oncoming gold or nickel atoms during sputter deposition. This could then account for the increased adhesion strength observed in gold-alumina and nickel-alumina couples above the melting threshold.[1] This means that the

adhesion strength is proportional to the number of gold or nickel atoms that can anchor onto the defective surface produced as a result of laser irradiation. Annealing the couples after sputter-deposition further improves the adhesion strength suggesting that further rearrangement of atom positions occurs opening up new sites for attachment of gold or nickel atoms.

In the case of fused silica too, an improvement in adhesion of gold-silica and copper-silica couples is observed again suggesting that some defects are created on the silica surface onto which the gold and copper atoms can attach. However, the increase in the adhesion strength is not so dramatic as in alumina. If increase in the adhesion strength is proportional to the number of bonding sites created, then the number of bonding sites created in silica is much less than that of alumina. Annealing the silica-copper and silica-gold couples also does not seem to affect the adhesion strength too much, suggesting that even after rearrangement, the number of bonding sites onto which the oncoming gold or copper atoms can anchor in the case of fused silica remains considerably less than in alumina.

Laser ablation takes place at higher energy densities. In the case of alumina, irradiated with 10 consecutive pulses, significant ablation takes place at energy densities higher than 2 $J/cm^2$ . Ablation starts after five pulses at 2 $J/cm^2$ , and at higher energy densities, the threshold number

of pulses required to initiate ablation decreases. [5] In the case of fused silica, ablation starts after pulses at 2 $J/cm^2$ . For both alumina and fused silica, the initiation of ablation appears to coincide with a drop in the adhesion strength of the studied metal-ceramic couples. Ablation causes explosive vaporization and removal of material of the near-surface region of the ceramic. This means that the melted zone, which is the possible source of defects is explosively removed from the substrate surface. The number of potential bonding sites available for oncoming gold, nickel or copper atoms thus, is greatly reduced. This leads to an observed drop in the adhesion strength with increasing laser energy density beyond the ablation threshold. Annealing of these metal-ceramic couples, causes a relative increase in adhesion strength at least in the case of alumina-gold and alumina-nickel. In the case of fused silica, annealing does not seem to have much effect on the observed adhesion strengths .

The oxygen content of the laser irradiation atmosphere also seems to affect the adhesion strength, especially in the case of alumina-gold and alumina-nickel couples. At 1 $J/cm^2$ , the adhesion strength of an 80 nm gold film on an alumina substrate laser treated in $Ar/H_2$ is 2 MPa. If the alumina substrate was laser treated in air, then the adhesion strength of the gold film rises to 30 MPa, and finally, if the substrate was laser treated in oxygen the adhesion

strength of the film is 50 MPa. When an alumina substrate is laser treated in a reducing atmosphere, F-centers or oxygen vacancies are created in the near-surface, thereby leaving an excess of Al in this region. This excess has been detected using XPS for alumina substrates laser treated in a reducing atmosphere.[12] Though laser treatment in the reducing atmosphere creates vacancies and interstitials, these bonding sites are not fully available for oncoming metal atoms. Therefore, a reducing condition during laser treatment does not greatly improve the adhesion strength. However, if laser treated in an oxygen rich atmosphere, the adhesion strength improves greatly. This is because, now the defective substrate is saturated with oxygen, and are now potential bonding sites for gold or nickel atoms. On annealing these couples, more bonding sites become available as a result of rearrangement, causing an even further increase in the adhesion strength of these couples.

In the case of fused silica, the irradiation atmosphere does not seem to greatly influence the adhesion strength. In fact, for both gold-silica and copper-silica couples, the adhesion strength does not vary greatly with the laser irradiation atmosphere. However, the highest adhesion strength obtained in the case of gold-silica was ~ 6 MPa for a silica substrate laser treated in oxygen at 2 $J/cm^2$ .

Measurements of adhesion of metal films vacuum deposited on glass and on silica surfaces have shown that,

for non-oxidisable metals such as gold, the adhesion strength remains constant at a comparatively low value, which can be completely explained in terms of Van der Waals' forces. [71] On the other hand, films of many oxidisable metals show an increase of adhesion with time and the final adhesion is generally one or two orders of magnitude greater than the adhesion of a gold film. A difference of this order suggests some kind of chemical bonding and it has been shown that the increase in adhesion is due to oxygen.[72] Results were obtained for iron films deposited on glass at different residual oxygen concentrations.[73] When the oxygen concentration during deposition was high, an increase in adhesion was found to occur with time. Even when the residual oxygen content during deposition was low, the adhesion still rose after deposition, though this time, the increase was much lower. The results were similar for aluminum films, which showed that films deposited at high residual oxygen concentrations showed high adhesion and the maximum values were reached before measurements could be made. At lower oxygen concentrations, the rise in adhesion was limited. Since, aluminum forms a protective oxide skin on exposure to air, the adhesion rose because of oxygen trapped within the film structure during deposition. When the film deposition was performed in a reducing atmosphere by working at low hydrogen pressures, thus substantially reducing oxygen during deposition, the adhesion of aluminum

films did not show any increase at all, and remained steady at a low value comparable with the adhesion strength of gold deposited on as-received substrates.

Thus, these results show that if an intermediate transition layer of oxide forms, the adhesion between a metal and an oxide surface can be enhanced.

## 5.2 Micro structure of Metallic Films Deposited on Ceramic Substrates

The SEM micro graphs are discussed in terms of surface tension effects and the thermodynamic work of adhesion. The work of adhesion, $W_{ad}$ , is related to the interfacial free energy by,

$$W_{ad} = \gamma_m + \gamma_c - \gamma_{mc}$$

where, $\gamma_m$ and $\gamma_c$ are the surface free energies of the metal and ceramic surface, respectively, and $\gamma_{mc}$ is the metal-ceramic interfacial free energy. In general, systems that have a higher work of adhesion also show high adhesion strength. Since the work of adhesion decreases as the interfacial free energy increases, systems with a high interfacial free energy generally also show poor adhesion strength.

Under equilibrium conditions, the three surface energies are related by Young's expression for the contact angle

$$\gamma_{mc} = \gamma_m \{ 1 + \cos ( \theta_{eq.} ) \}$$

When the contact angle is low, the metal film wets the ceramic substrate, and the interfacial surface energy is low, resulting in good adherence of the metal film onto the ceramic substrate. Poor wettability ensues from a high interfacial surface energy resulting in poor adherence. Therefore, low metal-ceramic interfacial energies are associated with good wetting and bonding tendencies and, hence, imply a more stable metal film free from agglomeration. Agglomeration results from poor wettability, causing pronounced aggregation and formation of globules in the metal film. Under these conditions, there is little true contact between the metal and the ceramic, and hence the adhesion is poor.

Many authors have tried to investigate the effect of oxygen on the wetting angle and the interfacial energies. Buttner, Funk and Udin [74] studied the change in surface tensions of solid silver in helium-oxygen atmospheres at several gas content ratios. They found that the surface tension of silver decrease linearly with the logarithm of the oxygen partial pressures. Humenik and Kingery [75,76] investigated different metal-ceramic systems in vacuum, hydrogen and helium. Nickel-alumina systems showed at least a thirty percent increase in the work of adhesion when measured in vacuum, over that measured in a hydrogen

atmosphere. Prominent interfacial reactions were observed in nickel-titania systems which show good wettability. This was evidenced by an abnormal decrease in the surface tension of nickel on titania and was attributed to the solubility of oxygen in the metal resulting from the dissociation of titania to a lower oxide, or Ti-$TiO_2$ solid solution. The chemical attraction between the metal and the oxide surface is considered to be the reason for the decrease in interfacial energy. The free energy change associated with wetting has been related to the formation of metal-oxygen bonds at the interface and to the free energy of formation of these bonds.

Alumina substrates were laser treated in $Ar/H_2$ , air and oxygen at 2 $J/cm^2$ . A 20 nm-thick gold film was sputter-deposited onto these substrates after laser irradiation. The gold-alumina couples were next annealed at 500°C for 45 minutes. They were then observed under a Hitachi S 800 scanning electron microscope. The gold film deposited on the substrate laser treated in oxygen was almost complete, indicating good wettability of the gold film on the alumina substrate, while the gold film deposited on the sample laser treated in $Ar/H_2$ had broken down into small agglomerates, showing poor wettability. This indicates that in the presence of oxygen, the wettability is improved, resulting in a lower interfacial free energy, $\gamma_{mc}$ . This stabilizes the gold film and prevents the pronounced agglomeration of the

gold film observed on the substrate laser treated in a reducing atmosphere. The decrease in the interfacial energy, in turn leads to an increase in the work of adhesion and hence in the adhesion strength, as confirmed by the pull-test results. This decrease can also be attributed to the formation of some kind of chemical bonding between the gold and the alumina in the presence of oxygen. The gold film deposited on the substrate laser treated in air, shows an intermediate morphology, exhibiting less agglomeration than in the film on the substrate laser treated in the reducing atmosphere, but still much more pronounced than in the film deposited on the substrate laser treated in oxygen. Thus, a direct relationship between the oxygen availability at the interface and the wettability as well as the adhesion strength has been proved.

Figures 4.15-4.19 show the morphology of a 20 nm thick gold-film sputter deposited on as-received alumina, laser-treated in air at 0.5,1,2 and 3 $J/cm^2$ . The gold film deposited on as-received alumina showed formation of larger number of islands, which were also smaller in size as compared to gold films deposited on alumina substrates laser-treated in air. At 1 $J/cm^2$ , the gold film showed much less agglomeration and better wettability. The gold film first appears to break at the original alumina grain boundaries, where the interfacial energy is higher and hence the work of adhesion should be lower than in the grain. Also, probably in the groove formed

by the two grains, the deposited film is much thinner. At laser energy densities higher than the melting threshold, the alumina substrate melts and resolidifies in a very short time, forming a smooth surface without grain boundaries. Therefore, the gold film has better wettability and forms less islands. However, at energy densities above the ablation threshold, large holes or craters are formed. Figures 4.18 and 4.19 demonstrate that there is no gold film around these holes formed as a result of explosive vaporization. This suggests that these holes act as "weak spots" with thinner metallic films (groove effect) and poor wettability. Thus, the adhesion strength shows a drop for energy densities above the ablation threshold.

## 5.3 In-situ Resistivity Experiments

The different parameters that play a role in these experiments are annealing time and temperature and thickness of the deposited gold film. Agglomeration effects have been found to be greatly enhanced at higher temperatures within a shorter time. It has also been found that for a particular thickness of film deposited on a substrate treated under a certain condition, agglomeration usually starts at a particular temperature, above which the film deteriorates rapidly, reaching a resistance on the order of mega-ohms. Below this temperature, the film remains stable for long periods of time, up to two days. The thickness of the gold

film also makes a major difference in their stability. A 200 ·A gold film deposited on an alumina substrate laser treated in oxygen at 1 J/cm$^2$ reaches a resistance on the order of Kilo-ohms after just annealing at 600 ·C for minutes, whereas a 600 ·A gold film deposited on a similarly treated alumina substrate reaches the same resistance after annealing at 650 ·C for minutes. It was therefore meaningful to compare films of similar thickness, that is, of close initial resistance values. Since, doubling of the resistance meant a film with only half the thickness, the initial film resistance was very critical in these experiments.

# CHAPTER 6

# CONCLUSIONS

1. The as-received adhesion strength of sputter deposited metal films of gold and copper onto polycrystalline alumina and amorphous fused silica is very poor.(< 0.1 MPa). The adhesion strength of as-received alumina-nickel couples is ~ 32 MPa.

2. Laser irradiation of both alumina and fused silica substrates significantly improves their adhesion to subsequently sputter deposited metal films.

3. There was a substantial improvement in adhesion in the case of alumina. The improvement in adhesion in the case of fused silica was much less substantial.

4. For alumina-gold couples, an increase in adhesion of over 500 times (to a maximum of ~ 50 MPa) that of the as-received adhesion strength was obtained.

For alumina-nickel couples, the maximum adhesion strengths obtained were above the limit of the testing apparatus. (> 80 MPa).

For gold-silica couples, an increase in adhesion of only 40 times (to a maximum of ~ 4 MPa) that of the as-received strength was obtained.

For copper-silica couples, an increase in adhesion of only 30 times (to a maximum of ~ 3 MPa) that of the as-received strength was obtained.

5. The adhesion strength is a strong function of the laser energy density. Initially, the adhesion strength increases with the energy density, until it reaches a maximum. Above this, a general decrease in adhesion strength is observed with energy density.

6. The functional dependence of adhesion strength on the laser energy density seems to be independent of either the laser irradiation ambient or the substrate or film material.

7. The rapid melting and solidification at the melting threshold produces lot of defects, e.g. vacancies and interstitials, on the substrate surface. The defective surface may contain sites where the metal atoms can be placed, thus accounting for the increase in adhesion strength at or below the melting threshold.

8. Ablation causes explosive vaporization and removal of material from the melted zone. This could remove some of the potential bonding sites available, thus accounting for the drop in adhesion strength observed at the ablation threshold.

9. The higher the oxygen content of the laser irradiation ambient the higher are the adhesion strengths obtained. Under a reducing atmosphere, F-centers or oxygen vacancies are produced, and the adhesion strength observed is low.

10. The effect of the oxygen content on the adhesion strength seems to be significant in the case of alumina. In the case of fused silica, the oxygen content of the laser irradiation ambient does not seem to have much effect on the adhesion strength.

11. In the case of alumina-gold couples, it is observed that higher oxygen content of the laser irradiation ambient also improves the wettability of the gold film to the alumina substrate, thus stabilizing the gold film. Pronounced agglomeration is observed in films deposited on substrates treated in reducing atmospheres.

12. Enhanced wettability of gold films deposited on alumina substrates laser treated in an ambient rich in oxygen, also suggests some kind of chemical bonding between the gold and the alumina, resulting in a decrease of the interfacial free energy, $\gamma_{mc}$.

13. Film break-up leading to subsequent agglomeration, seems to begin at surface imperfections of the ceramic, e.g. grain boundaries, etc, where the work of adhesion is likely to be lower than within the grain.

14. At the melting threshold, the ceramic substrate melts and resolidifies in a very short time, forming a smooth surface with the absence of grain boundaries. This results in a more stable metal film, with much less agglomeration.

15. Ablation causes formation of holes or craters, which are weak spots and which reduce the wettability of the metal film onto the ceramic substrate.

16. Post-deposition annealing seems to virtually double the adhesion strength, especially in the case of alumina-gold couples. Again, in the case of fused silica, this does not seem to have any great effect.

# REFERENCES

## REFERENCES

1. A.J.Pedraza, M.J.DeSilva, R.A.Kumar and D.H.Lowndes, The Adherence of Metallic Films to Laser Irradiated Alumina, to be published.

2. A.J.Pedraza and M.J.Godbole, Laser-Enhanced Sputter or Vapor Deposition of Thin Metallic Films on Ceramic Substrates, Metallurgical Transactions A, Vol 23 A, pp. 1095-1103.

3. David.B.Knorr, Mechanical Aspects of Mutichip Reliability, The Journal of the Minerals, Metals and Materials Society, July 1992.

4. A.J.Pedraza, Metal-Ceramic Bonding by Pulsed Laser Processing.

5. Douglas.H.Lowndes, M.J.DeSilva, M.J.Godbole, A.J.Pedraza, T.Thundat and R.J.Warmack, Smooth Polycrystalline Ceramic Substrates with Enhanced Metal Adhesion by Pulsed Excimer Laser Processing, Appl. Phys. Lett. 64(14), 4, 1994.

6. Douglas.H.Lowndes, M.J.DeSilva, M.J.Godbole, A.J.Pedraza and D.B.Geohegan, in Laser Ablation in Materials Processing : Fundamentals and Applications, edited by B.Brarem, J.J.Dubowski and D.P.Norton, Mater. Res.Soc.Symp.Proc., 285, Pittsburgh, PA, 1993, p 191.

7. J.T.Dickinson, L.C.Jenson, R.L.Webb and S.C.Langford in Laser Ablation : Mechanisms and Applications - II (Amer. Inst.of Phys. Conf.Proc.288, New York, NY,1993) , p 13.

8. J.E.Macdonald and J.G.Eberhart, Trans. Met. Soc. AIME, 233, 512 (1965).

9. W.A.Weyl, Adhesion and Adhesives - Fundamentals and Practice, J.E.Rutzler and R.L.Savage, Eds. John Wiley and Sons, New York, 1953, 36.

10. D.C.Moore and H.R.Thornton, J.Res.Natl.Bur.Std. 62,127, (1959).

11. D.M.Mattox, J.Appl.Phys.Letters, Vol.37, No.9, (1966).

12. A.J.Pedraza, J.W.Park, H.M.Meyer III and D.N.Braski,

13. H.L.Caswell and Y.Budo, J.Appl.Phys.Letters, Vol.35, No.3, Part 1, (1964).

14. Rao.R.Tummala, in Ceramic Substrates and Packages for Electronic Applications, Advances in Ceramics, Vol. 26, edited by Man.F.Yan, Koichi Niwa, Henry O' Bryan and Wayne.S.Young, 1989.

15. A.H.Kumar and R.R.Tummala, International Journal of Hybrid Microelectronics, 14, (4), 1991.

16. Bernard Schwartz, Ceramic Packaging of Integrated Circuits, Elect. Ceram., Vol. 3, No. 12, 1969.

17. Carl Zweben, Metal-Matrix Composites for Electronic Packaging, The Journal of the Minerals, Metals and Materials Society, July 1992.

18. M.Rothschild and D.J.Ehrlich, Journal of Vac. Sci. Technol. B 6, 1, 1988.

19. R.S.Taylor, L.E.Leopold, R.K.Brimacombe and S.Mihailov, Appl. Opt., 27, 3124, 1988.

20. M.V.Allmen, in Laser and Electron Beam Processing of Materials, Edited by C.W.White and P.S.Peercy, 1983.

21. Y.Hsia, The Journal of the Minerals, Metals and Materials Society, July 1992.

22. Martin von Allmen, Laser - beam Interactions with Materials, edited by Aram Mooradian, Springer-Verlag, 1987.

23. Pedraza A.J., in Laser Materials Processing III, edited by J.Mazumder and K.N.Mukherjee, 183, 1989.

24. A.J.Pedraza, M.J.Godbole, D.H.Lowndes and J.R.Thompson, Journal of Vacuum Science and Technology A, 6(3), 1763, 1988.

25. Y.Shimada, "Large, multilayer glass-ceramic substrates for Supercomputers", IEEE Trans. Components, Hybrids and Manufacturing Technology, CHMT-9, 1986.

26. A.D.Westwood and M.R.Notis, The Journal of the Minerals, Metals and Materials Society, June 1991.

27. B.C.Johnson, "Overview of High Performance Packaging Materials", ibid.

28. N.Kuramoto, H.Taniguchi and I.Aso, "Translucent AlN Ceramic Substrate", IEEE Trans. Components, Hybrids and Manufacturing Technology, CHMT-9, 1986.

29. J.L.Sprague, "Multilayer Ceramic Packaging Alternatives", IEEE Trans. Components, Hybrids and Manufacturing Technology, CHMT-13, 1990.

30. L.E.Murr, Interfacial Phenomenon in Metals and Alloys, Addison-Wesley Publishing Company, London, 1975.

31. E.D.Hondros, "Bonding of Metal/Ceramic Interfaces", Science of Hard Materials, E.A.Almond, edited by C.A.Brooks annd R.Warren, Adam Hilger Ltd., Bristol, 1986.

32. R.J.Good, Adhesion Sci. and Tech., Vol. 9A, edited by Lieung-Huang Lee, Plenum Press, New York, 1975.

33. M.D.Pasley, J.B.Pethica and D.Taylor, "Adhesion and Micro-mechanical Properties of Metal Surfaces", Wear, 100, 1984.

34. J.E.E.Baglin, Ion-beam Modification of Insulators, edited by Paula Mazzoldi and W.A.George, Elsevier, Amsterdam, 1987.

35. B.N.Champan, Glow Discharge Processes, John Wiley, New York, 1980.

36. J.E.E.Baglin, Thin Films: The Realtionship of Structure to Properties, edited by C.R.Aita and K.S.Sreeharsha, Materials Research Society, PA, 1985.

37. S.V.Pepper, Journal of Appl. Phys., Vol. 47, 3, 1976.

38. S.V.Pepper, Journal of Appl. Phys., Vol. 50, 12, 1979.

39. M.M.Karnowsky and W.B.Estil, The Rev. of Sci.Instr., Vol. 35, 10, 1964.

40. M.P.Borom and J.A.Pask, J. Am. Ceram. Soc. , 49, 1, 1966.

41. P.Benjamin and C.Weaver, Proc. Roy. Soc. (London), A 261, 516, 1961.

42. L.Holland, The Properties of Glass Surfaces, John Wiley and Sons, New York, 1964.

43. T.E.O'Brien and A.C.Chaklader, J. Am. Ceram. Soc. , 58, 8, 1974.

44. G.Katz, Thin Solid Films, 33, 1976.

45. J.F.Burgess, C.A.Neugebauer, G.Flanagan and R.E.Moore, Solid State Technol., 1975.

46. H.D.Keith, Proc. Roy. Soc. (London), 69B, 180, 1956.

47. S.P.Murarka and M.C.Peckerar, "Electronic Materials: Science and Technology", Academic press Inc., 1989.

48. L.I.Maissel, R.Glang, "The Handbook of Thin Film Technology", McGraw Hill, NY, 1970.

49. K.L.Mittal, Electrocomp. Sci. Technol., 3, 21 (1976).

50. K.L.Mittal, in Adhesion Measurement of Thin Films, Thick Films, and Bulk Coatings, edited by K.L.Mittal, ASTM Spec. Tech. Publ. 640, ASTM, PA, 1978.

51. B.N.Chapman, J. Vac. Sci. Technol. 11,106, 1974.

52. D.S.Lin, J. Phys. D 4, 1971.

53. K.Kuwahara, H.Hirta and N.Umemoto, in Adhesion Measurement of Thin Films, Thick Films, and Bulk Coatings, edited by K.L.Mittal, ASTM Spec. Tech. Publ. 640, ASTM, PA, 1978.

54. K.S.Kim and J.Kim, J. Eng. Mater. Technol., 110, 266, 1988.

55. K.S.Kim, in Mater. Res. Soc. Symp. Proc., 1988 Spring meeting, Symposium F : Adhesion in Solids, edited by D.M.Mattox, C.Batich, J.E.E.Baglin and R.J.Gottschall, Pittsburgh, PA, Vol. 119.

56. R.Jacobsson, Thin Solid Films, 34, 191, 1976.

57. R.B.Belser and W.H.Hicklin, Rev. Sci. Instrum., 27, 293, 1956.

58. D.W.Butler, J. Phys. E., 3, 979, 1970.

59. W.H.Dancy, Jr. and A.Zavarella, Plating 52, 1009, 1965.

60. S.Moses and R.K.Witt, Ind. Eng. Chem., 41, 2334, 1949.

61. P.Laeng, P.A.Steinmann and H.E.Hintermann, Oberflaeche Surf. 23, 108, 1982.

62. O.S.Heavens, J. Phys. Radium 11, 355, 1950.

63. C.Weaver and R.M.Hill, Philos. Mag. 3, 1402, 1958.

64. P.Benjamin and C.Weaver, Proc. Roy. Soc. (London), A 254, 163, 1960.

65. A.J.Perry, P.Laeng and H.E.Hintermann, in Proceedings of the 8th International Conference on Chemical Vapor Deposition, Electrochemical Society, Pennington, NJ, 1981.

66. P.Laeng and P.A.Steinmann, in Proceedings of the 8th International Conference on Chemical Vapor Deposition, Electrochemical Society, Pennington, NJ, 1981.

67. H.E.Hintermann, P.Laeng and P.A.Steinmann, in Proceedings of the International Ion Engineering Congress, ISIAT '83, Japan, 1983.

68. J.Valli, U.Makela, A.Matthews and V.Murawa, J. Vac. Sci. Technol., A, 3, 2411, 1985.

69. J.Sekler, P.A.Steinmann and H.E.Hintermann, Surf. Coat. Technol., 36, 519, 1988.

70. M.J.DeSilva, Ph.D. Proposal , University of Tennessee, Knoxville, 1994.

71. C.Weaver, in Proc. First Int. Conf. on Vacuum Techniques, Namur. London : Pergamon Press, 1960.

72. P.Benjamin and C.Weaver, Proc. Roy. Soc. A., 254, 197, 1960.

73. P.Benjamin and C.Weaver, Proc. Roy. Soc. A., 261, 516, 1961.

74. F.H.Buttner, E.R.Funk and H.Udin, J. Phys. Chem., 56, 1952.

75. Micheal Humenik and William.D.Kingery, J. of the Amer. Ceram. Soc., 34, 10, 1952.

76. B.S.Ellefson and N.W.Taylor, J. of the Amer. Ceram. Soc., 21, 6, 1951.

# VITA

Rajagopalan A Kumar, was born in Tamil Nadu, India on October 22 nd, 1970. After graduating high school from Kendriya Vidyalaya, Calcutta in May 1988, he joined the Indian Institute of Technology at Kharagpur. He received a B.Tech. (Hons.) degree in Metallurgical Engineering in July, 1992.

In August 1992, he joined the University of Tennessee, Knoxville, Materials Science and Engineering for working towards his Masters. He plans to pursue his Ph.D. in the Dept. of Management Science at UT, Knoxville.